Upscaling soil and vegetation measurements in an alpine catchment using remote sensing and statistical modelling

MSC THESIS

Author: D. Haagmans (6610633)
Supervisors: P. Kraaijenbrink and W. Immerzeel
Date: 08/12/2023

Aerial image of the Meretschibach catchment in July 2023, in the Swiss Alps.

Utrecht University
Faculty: Geosciences
MSc: Earth, Surface and Water

Utrecht University

ABSTRACT

Soil texture is an important soil physical property that determines water availability, nutrient availability and growth of vegetation. The growth of plant species and development of high-alpine soils are shifting in alpine catchments due to changes in conditions as a result of e.g. warming at higher elevation, shorter periods of snow cover and less precipitation falling as snow. Hence, understanding hydrological behaviour in high alpine catchments is crucial. Therefore, insight in the spatial distribution scale of soil texture and vegetation in an alpine catchment is required. In this research, field data obtained during 3 weeks of fieldwork in the Meretschibach catchment was used in combination with remotely sensed data for statistical modelling. The Random Forest model was used to predict soil textures and vegetation classes on a catchment scale including accuracies and variable importance for all models. The soil textures in the study area both determined and predicted were dominated by high sand fractions: sandy loam, loamy sand and sand. The most important variables for prediction of soil properties were slope and elevation. In contrary, the most important variables for predicting vegetation and rock cover percentage on surface were spectral bands and NDVI. The RF classification model for predicting vegetation showed the best performance and poorer performance for soil textural classification with a misclassification rate of 19.5% and 61.1% respectively. The performance of RF regression model was most accurate for prediction of rock cover percentages with an R^2 of 0.57 and a NRMSE of 0.17. The results demonstrate that field data in combination with RF models can be used to determine the spatial distribution of surface characteristics. However, it suggests that discovering statistical trends for in-soil parameters is challenging. The findings did suggest that there is potential in narrowing the training data to the most important prediction variables. Future research could also use different models to see which model is superior for upscaling soil texture for this specific site.

TABLE OF CONTENTS

1. INTRODUCTION

1.1 THE GREENING OF ALPINE REGIONS DUE TO CLIMATE CHANGE

Effect of climate change on hydrology and ecology

The colonization of new species has accelerated during this century in the European Alps (Steinbauer et al., 2018), revealing change in ecosystems. The vegetation zone belts in mountainous ecosystems are shifting upwards. The vegetation zones represent climate conditions where specific plant species will thrive. Therefore, shifts in vegetation type provide evidence for climate change impact on mountainous ecosystems (Hagedorn et al., 2019). The European Alps experience greening (Beniston, 2012; Choler et al., 2021; Hagedorn et al., 2019; Körner, 2021; Rumpf et al., 2022; Steinbauer et al., 2018; Viviroli et al., 2011). According to Rumpf et al. (2022), 77% of the Alpine areas above the tree line undergo greening over the last four decades. Also, tree lines are advancing to higher altitudes at 52% of the 166 sites discussed by Harsch et al. (2009).

Field Code Changed

Climate change has a great impact on ecology and hydrology in alpine catchments. The general retreat of mountain glaciers is already perceptible through the last decades. An increase in temperature of 2 °C since 1900 is arising at high elevations in the European Alps (Beniston, 2012). Regional climate models including different greenhouse-gas emissions scenarios suggest that winters in Switzerland may warm up to 3-5 °C and summers by 6-7 °C by 2100 (Beniston, 2012). The greening of the alpine areas occurred predominantly in warmer areas of the Alps experiencing strong winter warming (Harsch et al., 2009; Rumpf et al., 2022). The precipitation is projected to increase in winter, (Beniston, 2012; Rumpf et al., 2022), suggesting that the average snowline will rise by 150 m for each warming degree indicating that the possible snowline could shift 450-750 m (3-5 °C) upward during winter. This upward shift of the snowline reduces precipitation falling as snow, leading to a snow mass reduction in the European Alps (Rumpf et al., 2022). According to the study of Viviroli et al. (2020), it is projected that approximately 1.5 billion people (24% of the world's lowland population) will have a critical reliance on runoff originating from mountains by 2050 assuming a moderate scenario. Therefore reduced snow mass and melt has a direct impact on people living downstream that are dependent on freshwater resources.

Despite warmer temperatures during spring, vegetation development in alpine and sub-alpine belts (>1800 m) is still hindered by snow until late spring. As a result, greening in these alpine regions primarily acts during summer and autumn (Filippa et al., 2019). In alpine catchments, sparsely vegetated areas like screes, talus and glacial forelands can potentially be invaded with pioneer species due to changes in climatic conditions (Choler et al., 2021). The pioneer species in sparsely vegetated areas contribute to a feedback loop between snow and vegetation, since the growth of species will trap blowing snow and increase radiation exchange resulting in faster snowmelt and reduced snow cover (Mazzotti et al., 2021; Sturm et al., 2001). Therefore, an increase in vegetation and a decrease in snow cover seems to contribute to the alpine snow mass buffer decrease during winter.

The effect of climate change on alpine regions will impact generation of hydropower, agriculture, natural habitats, (glacial) tourism and also an increase of potential natural hazards impacts inhabitants but also leaves an indirect impact on insurance companies (Beniston, 2012; Salim et al., 2021). Water supply changes influencing hydropower generation and therefore energy supply. The productivity for agriculture will change when water supply changes. The consequences of the greening and glacial retreat for tourism include issues related to proposed activities and attractiveness of a site, itineraries and glacier access (Salim et al., 2021). The thawing of permafrost may cause rock falls and landslides

due to changes in physical properties of the ground, increasing the risks of natural hazards. Also, thawing of permafrost might release greenhouse gases and will result in loss of specific habitats (Rumpf et al., 2022). All these discussion points are related to change in morphology, vegetation, hydrology and soil development in these alpine zones. Therefore understanding these relations between terrain characteristics, ecology, soil properties and hydrology by upscaling spatial data on alpine catchments is crucial.

Impact on high elevation soil development

A schematic sketch on the soil-vegetation-elevation relation is shown in Figure 1. In the boundaries of this research, less attention given to the underground fungi and bacteria and the focus will lay on the soil, hydrology, vegetation and terrain relation. The soil texture will be different for zones with larger vegetation and deeper soil structures compared to zones where there is only grass with relatively small root systems. A shift in vegetation and soil texture will indirectly indicate a shift in alpine underground ecosystems and vice versa.

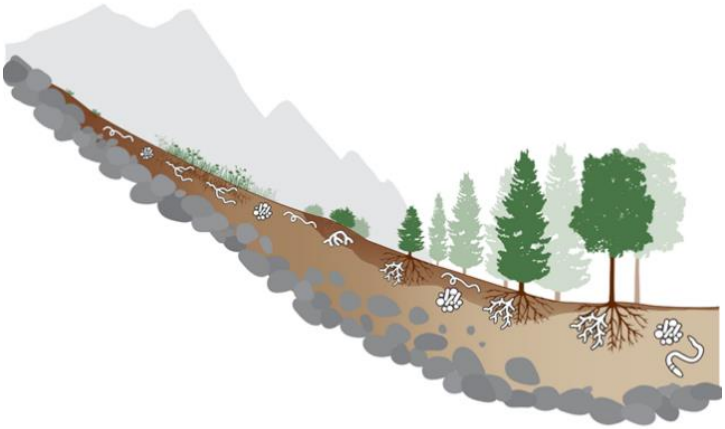

Figure 1: A sketch of mountain ecosystems above and below the ground. The legend already describes the belowground organisms. The aboveground vegetation represents from right to left: deciduous forest, large coniferous forest, smaller coniferous forest, shrublands, grasslands, bare soil. Image adapted from Hagedorn et al. (2019)

Soil development on high elevation soils change as the environmental conditions change for certain elevations. Yet, the process of soil formation in high altitude regions is challenging. Insufficient water retention and low nutrient availability in poorly developed, high elevation soils can limit the expanses of specific species that have the potential to advance upward (Henne et al., 2011), resulting in other specific species that are more likely to advance.

On higher elevations bare rocks, climate conditions and erosion play a vital role and can hinder soil development. Nevertheless, the soil organic matter (SOM) build-up in topsoil of glacier forelands is proceeding at the global scale (Khedim et al., 2021). The previously barren rock surfaces, once covered in ice and snow, are now becoming conducive to the growth of plant species and the habitation of various organisms. For example, an upward shift of the forest in the Ural mountains leads to changes in soil organic material (SOM) quality, an increase in net nitrogen mineralization and accelerates carbon cycling, which in turn may stimulate vegetation to grow and increasing carbon sequestration in biomass (Kammer et al., 2009). A benefit of the high-elevation soil development is the gain of carbon in early successional ecosystems (Hagedorn et al., 2019).

1.2 Pedogenic variables in Alpine environments

The shifts in hydrology, soil properties, vegetation and terrain in mountainous areas should be monitored and analyzed to understand this everchanging landscape. However, field measurements and trips to high elevation areas come with high costs. Since these changes in hydrology are critical for a lot of people and many countries rely on freshwater resources from mountainous areas it is important to expand our knowledge on mountainous hydrologic behavior, including soil and vegetation changes. This can potentially be achieved by using remotely sensed data to predict pedogenic variables, hydrologic parameters and classify vegetation. When prediction by UAV or satellites becomes more reliable the field costs could potentially be less and time management could be more efficient.

The input parameters for prediction modelling may vary for each predictive variable. The parameters derived from satellite or UAV imagery are topography, terrain attributes and hydrological parameters. Landscape topography is an important factor when considering landscape distribution of soil variables since it impacts the transport of water and nutrients through overland and lateral flow. From UAV imagery multiple terrain attributes can be derived with high-resolution DEMs (Digital Elevation Models). Imagery alone is sometimes already sufficient to build a reasonable model mapping soil organic carbon (SOC), its relative importance was 65% compared to 20% climate variables and 15% topography (Yang et al. 2021). Probably because of the strong dependence of SOC on native vegetation intensity and environmental covariables derived from primary DEM terrain analysis (including elevation, profile and plan curvature, slope angle, aspect and position).

Besides, there are secondary terrain attributes that are often of indirect impact on soil property prediction. Several studies have used secondary terrain attributes representing hydrological processes on soil development. Secondary attributes like upslope contributing area, topographic wetness index (TWI), stream power index (SPI) and accumulated flow index (Bishop & Minasny, 2006) may strengthen prediction models. The TWI characterizes the flow of water across a landscape. Higher TWI values suggest wetter conditions and vice versa with drier conditions. Wetter conditions may suggest more erosion and sediment deposition which impacts soil texture. The SPI is used to quantify and analyse the energy of flowing water within a river or stream. Therefore this index takes into account different factors, including streams discharge and gradient of the stream channel. Accumulated flow is influenced by precipitation, runoff, inflow from tributaries and losses due to evaporation and infiltration and represents the total amount of water that flows through a particular point over a specified period of time.

Moore et al. (1993) found that both slope and the TWI are the terrain attributes that correlate most highly with surface soil attributes. In addition, Li et al. (2020) also subjected the TWI as the most influential topographic metric on Soil Organic Carbon density and increasing SOC density often correlates with an increase in clay and silt content, thus changing soil texture. Furthermore, the saturated hydraulic conductivity (k_{sat}) dictates how water moves within the soil, ultimately influencing the dispersion of soil moisture and, consequently, the availability of water for plants (Maier et al., 2020). The TPI shows whether a position is higher or lower than its surroundings and can therefore be of indirect influence on soil texture due to water flow, erosion, sediment deposition and soil development. The TRI values correspond to terrain steepness, higher values means steeper terrain. Therefore has an impact on the potential of sediment distribution.

1.3 MODELLING METHODS FOR PREDICTING PROPERTIES ON CATCHMENT SCALE

Digital maps of field data can be developed using statistical models. Statistical models use input or training data to predict data. Field data can be used for construction of a model and also for validation of the model. There are several models to estimate field data from spatial terrain analysis. For example, in the research of Ließ et al., (2012) two methods were applied to estimate terrain parameters including kriging and the mean value method (Inverse distance weighing). Kriging is a spatial interpolation method used to estimate parameters at unobserved locations and kriging also provides an estimate of the uncertainty associated with the prediction. The mean value method is a simpler technique relies on a weighted average of the values nearby an unobserved location. This method is therefore useful when there is limited amount of data available. For Ließ et al., (2012) the mean value method performed best, probably because of the small size of the dataset.

Kriging can be subdivided into multiple variants. Li et al. (2020) used Ordinary Kriging (OK); analyses of spatial relations (field sample data) for estimation of soil organic carbon (SOC). OK is only a valid method for soil texture predictions with a large dataset of field measurements (Li et al., 2020). However, ordinary kriging does not include covariation when predicting soil variables from terrain attributes (Odeh et al., 1995). Hence, to overcome the ordinary kriging limitations regression is often combined with kriging (RK) for better performance (Li et al., 2020; Odeh et al., 1995). However, these techniques are limited as the prediction could only be based on continuous variables.

Likewise, predictions of soil properties can also be achieved by machine learning (ML) techniques, for example tree-based methods. Multiple tree-based methods are widely used already (Farooq et al., 2022; Ließ et al., 2012; Pahlavan-Rad et al., 2020; Peters et al., 2007; Pouladi et al., 2019; Veronesi & Schillaci, 2019). Regression tree (RT) and Random Forest (RF) are tree-based models that can assign particular soil parameters to typical landscape positions. The RT and RF models use machine learning techniques and are known as a popular classification algorithm and relatively easy to understand and interpret.

RT models are only based on one decision tree. The one decision tree splits into binary nodes with one predictor variable and therefore this tree contains multiple decisions. RT model is relatively simple and can be limited in predictive performance and prone to overfitting. RF models are based on multiple decision trees. The multiple decision trees reduce overfitting and have stronger generalization capacities (Karabadji et al., 2023). A RF model will be less sensitive to the original training data as it uses bootstrapping which ensures that the same data will not be used for every tree. The random feature selection helps to reduce the correlation between the trees.

Several studies already used RT models and RF models to predict soil properties. For instance: McKenzie & Ryan (1999) used RT model for spatial predictions of soil variables by using digital terrain and gamma radiometric survey data as explanatory data. Peters et al. (2007) applied a multiple linear regression model and a RF model to predict ecohydrological distributions of groundwater-dependent vegetation types in Belgium. Pahlavan-Rad et al., (2020) implemented the multiple linear regression and RF models for soil water infiltration in a dry flood plain in eastern Iran. Ließ et al. (2012) used both RTs and RF models as statistical models to predict spatial distribution of soil texture from terrain parameters. Multiple studies reveal that RF models optimize the outcome compared to other tree-based models applied in the study (Ließ et al., 2012; Pahlavan-Rad et al., 2020; Peters et al., 2007; Prasad et al., 2006). Therefore, in boundaries of this research it is expected that the soil parameter prediction based on Random Forest models will have the potential to estimate field parameters based on a moderate to large dataset.

Furthermore, random forest models are a promising technique to predict soil properties because of covariation in field data. In addition, prediction of both nominal as continuous variables can be constructed by using RF models. In combination with terrain attributes, hydrologic parameters and vegetation inputs the decision trees will be larger and potentially decrease the uncertainty for the random forest model.

The prediction uncertainty is crucial for every statistical modelling method. In the research of Takoutsing & Heuvelink (2022) the prediction uncertainty for continuous variables was less accurate for machine learning algorithms than for regression kriging. However, in the study of Song et al. (2021) the RF model shows a higher accuracy for the prediction of pressure ulcer compared to SVM, ANN and RT models. The prediction uncertainty can be determined by using the coefficient of determination (R^2) and the Root Mean Square Error (RMSE) for RF regression modelling (Chicco et al., 2021). For RF classification models, the prediction uncertainty can be determined by determination of the out-of-bag (OOB) Brier score, AUC and a confusion matrix (Brier, 1950; Farooq et al., 2022; Ishwaran et al., 2021).

1.4 Research gaps and aim of this study

Climate change is contributing to the upward shifts in vegetation and earlier annual snowmelt in alpine regions. As a result, soil texture could potentially change resulting in different hydrological behaviour of alpine regions. Important hydrological factors like run-off, infiltration capacity and water uptake by root systems impact the local environment. Therefore, to expand knowledge on high-elevation catchments it is crucial to apply field measurements and spatial analyses. This study will narrow the knowledge gap on high-elevation soil property prediction and discusses multiple ways to estimate field parameters on catchment scale based on sampling and UAV imagery. Statistical models will be used for prediction of both classified and continuous data.

This yielded the following main research question and several sub questions:

- **What is the spatial distribution of soil properties and vegetation in the Meretschibach catchment?**
- *How are these soil properties linked to terrain characteristics?*
- *How could field data and UAV imagery be applied to estimate soil properties?*
- *What field parameters could be accurately predicted by statistical modelling?*
- *What variables have the greatest impact on soil and vegetation predictions on a high elevation area?*

2 STUDY SITE AND METHODS

2.1 MERETSCHIBACH CATCHMENT, SWITZERLAND

This study contributes to this research gap by implementing field research in an alpine catchment in the Swiss Alps. The Meretschibach catchment is a small catchment of the Rhone river located in the southwestern Swiss Alps. The Meretschibach catchment is about 9 km^2 and stretches from Bella Tolla mountain peak (3025 m) northward toward the Rhone valley (600-700 m). The study area ranges from Bella Tolla till past the treeline and has its border at ~1800 m where patches of forest are already present representing the upper half of the Meretschibach catchment (Figure 2). Frank et al. (2017) modelled debris-flow at the lower part of the Meretschibach catchment. Not any research has been done in the upper part of the catchment yet. The upper part of the Meretschibach catchment has a yearly mean precipitation rate of 80 mm per month and has a mean maximum temperature of 8° C and a minimum temperature of 1° C over the period 2010 till 2022 (Appendix 14). Also, a small glacial remnant (Bella Tolla glacier) is present near the top of the study area on a northward facing slope. The basins and slopes are covered with older and younger moraines and debris slope deposits; in addition a rock glacier covers a large part of the middle basin. Three lakes are present; Oberer Märetschisee, Unterer Märetschisee and the smaller lowest two are nameless. There are two anthropogenic factors; hydropower dams at all three lakes and grazing by cows; dominant in the morphology and ecosystems of the landscape. The lakes are used for generation of hydropower.

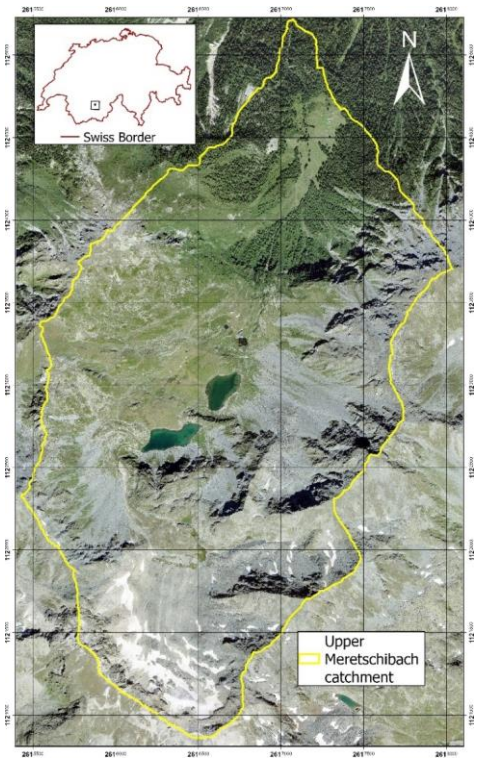

Figure 2: The outline of the upper part of the Meretschibach catchment

2.2 Acquisition of UAV imagery

2.2.1 UAV characteristics

A fixed-wing UAV eBee X (Figure 3) was used for mapping and surveying applications. Similarly, UAV's of the eBee series were widely used in previous studies for mapping of alpine regions (Gaffey & Bhardwaj, 2020; Ramsankaran et al., 2021; Revuelto et al., 2021). The eBee X UAV has a wingspan of 116 cm and a maximum take-off weight of 1.6 kg. A maximum flight time of 40 minutes was considered (to remain in the safe zone of battery). The nominal coverage of this UAV is smaller than the Meretschibach catchment area. Therefore, multiple flights missions were carried out.

The UAV's wind resistance is up to 46 km/h and UAV missions were only performed when there was no precipitation. The UAV contains a MicaSense RedEdge-MX sensor measuring the visual as well as red edge and near-infrared bands and the UAV has a Ground Sampling Distance (GSD) of 8 cm per pixel on 120 m height. The eBee X UAV collects data during a flight using this sensor and a Global Navigation Sattilite System (GNSS) receiver. This raw GNSS data was corrected by using data from a base station and therefore post-processed after the flights. The Post-Processing Kinematic (PPK) technique was used to improve the accuracy of the geospatial data and to georeferenced the imagery. The collected GNSS data was PPK corrected by using the Continuous Operating Reference Station (CORS) installed in Leuk, Switzerland (HOH2).

*Figure 3: Fixed-Wing UAV eBee X (*eBee X Mapping UAV - Drones*).*

2.2.2 UAV flight missions

Multiple UAV flights were performed at the Meretschibach catchment in Switzerland. The planning and construction of the flight missions was done by using the eMotion 3 software. A simplified planning of a flight mission features a take-off, a selected area that could potentially be covered by the UAV and an optimal landing spot. The take-off of a UAV eBee X mission was done by holding the UAV and releasing it after activation of a flight mission. In contrast, an ideal landing spot has to be somewhere on surface. Ideal landing positions are relatively flat areas covered with grass with no rocks on the surface. The selection of optimal take-off and landing spots is vital to minimize the risks correlated with take-off and landing on steep slopes and debris.

The aim of the UAV flight missions was to capture the entire upper Meretschibach catchment. However, due to UAV malfunction, the resulting area covered by UAV missions was subsequently reduced. The UAV experienced a crash after several missions. Consequently, the study area for parameter prediction now extents to the region that had been covered by the UAV up to that point, see Figure 4. The grid cell size was depicted at a size of 4x4 meters. As a result, the area covered by the UAV contains 77136 cells. This results in a study area of approximately 1.23 km^2. The study area

includes the Unterer Märetschisee and two small lakes near the hydropower company. These lakes are clearly visible in the southwest corner on the high resolution orthophoto (10x10 cm) derived from the flight missions (Figure 4). Therefore, parameters calculated for these waterbodies are excluded as they do not represent valid predictive data.

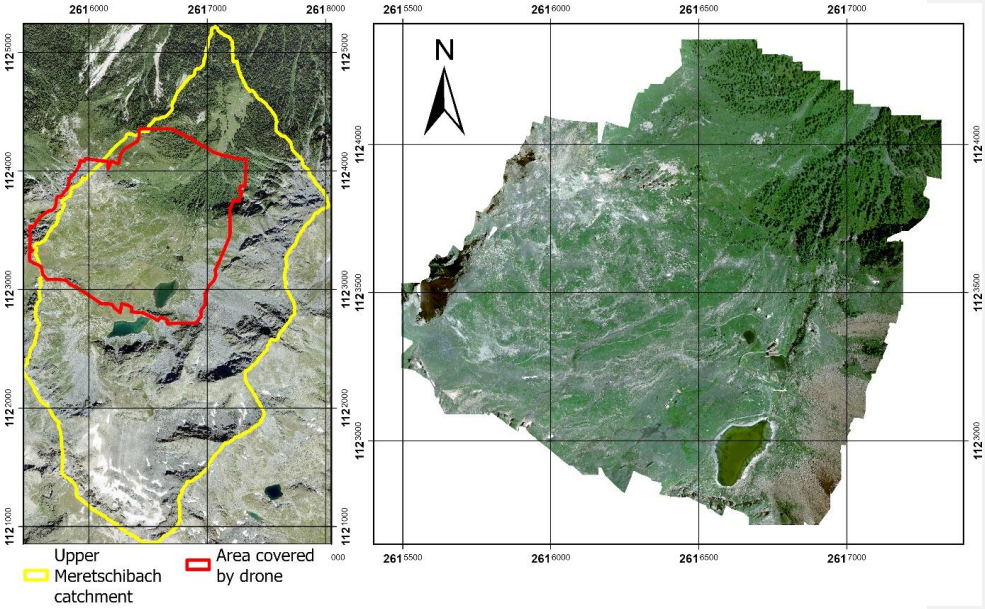

Figure 4: The completed UAV flights during fieldwork in the Meretschibach catchment, background are RGB bands derived from Sentinel-2 and the orthophoto on the right image is high-resolution orthophoto obtained from the UAV missions.

2.3 Acquisition of ground measurements

Two types of ground measurements were conducted in this research: purckhauer measurements and the establishment of plots. The primary focus of this research was achieving a large database of specific soil, vegetation and surface parameters. The purckhauer measurements imply fewer measured variables of soil properties and vegetation descriptions and exclude hydrological parameters. Therefore, these measurements were less time consuming in comparison to the establishments of plots.

The plots involve more extensive measurements, providing detailed descriptions of vegetation, soil properties (horizon, color, organic matter) and hydrologic measurements at fewer locations divided in different vegetation belts. The plots were established for research in microtopography, hydrology, vegetation and soil properties in different vegetation belts. Van de Lisdonk (2023) studied the relation between hydraulic and physical properties of alpine soils concerning terrain properties and vegetation at these plot locations.

For the scope of this research, further elaboration of plot measurements was exclusively focused on plot location parameters that were also measured at purckhauer locations.

2.3.1 Purckhauer measurements

After completion of the UAV missions the outline of the study area was clear. Several parameters were measured in boundaries of this study area. For instance: soil texture, soil depth, organic matter depth and rock fragments in soil. A purckhauer tool was employed to measure soil depth, depth of organic matter and to determine the soil texture. The purckhauer has a length of 101 cm which in turn will be the *minimum* soil depth when this depth is reached at a certain point. The purckhauer had the shape of a large pin and was driven into the ground using a sledge hammer (Figure 5A & C). A mechanical extraction tool is necessary to allow easy extraction at difficult environments (Figure 5B). Alpine soils often contain rock fragments and a purckhauer is recommended for alpine soil measurements as it has the potential to penetrate small pieces of rock.

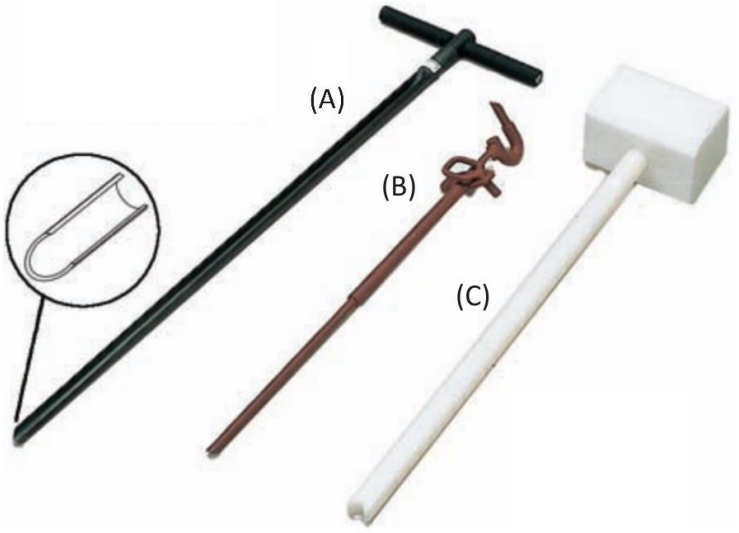

Figure 5: (A) is purckhauer with core, (B) is mechanical extraction tool and (C) is a large synthetic hammer. Image adapted from Skaling (2008).

The purckhauer (Figure 5A) is smashed into the soil until a certain depth is reached which is noted as the soil depth. A tape is used on the purckhauer to indicate soil depth while extracting the purckhauer. The purckhauer features a core (Figure 5A) where soil particles might adhere, allowing for the measurement of both soil texture and the presence and depth of organic layers (if present). Soil texture was determined in the field using a standardized soil determination flowchart (Appendix 1). The determined soil texture consist of different sand, silt and clay percentages. The proportions could vary within a classified soil texture as visible in the U.S. Department of Agriculture (USDA) textural triangle (Figure 6). To tackle this variation a strategy was used based the standardized flowchart (Appendix 1). For instance, if a sandy clay felt smoother, it might contain a higher clay content compared to a coarser sandy clay. As a result, all percentages of sand, silt and clay were also recorded for each purckhauer measurement.

Furthermore, vegetation type was observed at each purckhauer location. Vegetation types were described within various vegetation classes and within these classes specific species were identified and recorded. The specific species within a class include different species of tree, shrub, grass and herbs. However, for simplification all specific species are classified and in boundaries of this research

only the classified vegetation was treated. The vegetation classes included: Forest, Shrubs, Grass and Bare areas (vegetational cover below 15% (Anderson, 1976)). Since purckhauer measurements could not be performed in areas with bare soil, descriptions of bare soil areas were not included in the purckhauer database.

In addition, other surface properties as rock surface cover, slope and aspect were determined at all locations. Rock surface cover was estimated on a 1 by 1 meter scale around the hole created by the extraction of the purckhauer. An estimation diagram was used based on rock size and percentages for in-field estimation (Appendix 2). Slope and aspect were both measured by using a slope measurement tool and a compass (Appendix 3).

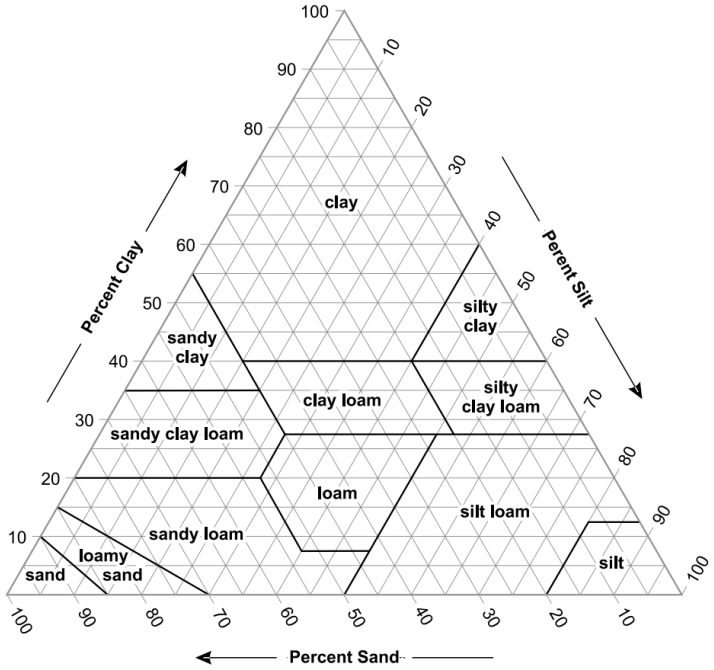

*Figure 6: USDA textural triangle including percentages of sand, silt and clay for 12 different textural classes (*Soil Survey Manual, 2017*)*

2.3.2 Plot construction

The measurements at plots consist of surface characteristics, vegetation descriptions, soil profile descriptions (up to 30 cm) and hydrological parameters.

Rock cover percentage and vegetation were described at each plot. Rock cover percentage was estimated by using a rock cover estimation diagram of rock size and percentages (Appendix 2). Vegetation descriptions classification was done by identifying different species in the field. A plot vegetation description comprises of both plant recognition and classification of dominant vegetation present (with aerial photographs as back-up). In support of on-site vegetation descriptions and to enhance data reliability, photographs were taken at all plot locations. In this research, rock cover percentage and vegetation class were both applied in statistical modelling.

If possible, soil profile and soil moisture was measured and described at three different depths (e.g. 5, 10, 30 cm). This was done by excavation of holes near the plot. Each plot comprises a general profile description. A general profile description of e.g. the upper 30 cm (if possible) was made in pits close to the vegetation plot, describing horizons, texture, colour and depth. Soil texture was estimated based on the estimation protocol to classify soil texture in-field (Appendix 1). Undisturbed soil samples were taken from the shallow soil in proximity to the plots (10 cm depth, 3 per plot) as well as for 3 depths for those with a moisture profile for the soil hydraulic properties.

The soil samples taken at the plots were brought back to the University of Utrecht for further analysis. Here the ksat, infiltration capacity and SOM will be measured using various methods (van de Lisdonk, 2023). In boundaries of this research, only the measured ksat values were used as a potential hydrological prediction parameter. The ksat measurements in the UU Lab were performed using a permeameter and elaborately discussed by van de Lisdonk (2023). The Ksat holds significance as it governs surface infiltration rates and the lateral and vertical movement of water within the soil. An increase in vegetation cover is expected to increase microporosity and thus increase Ksat (Maier et al., 2020).

Van de Lisdonk (2023) determined ksat by using Darcy's Law (Hendriks, 2010). Therefore, determination of the pressure head (dh) and travel distance (dx) was necessary. The water of volume passing through the sample in a specific timeframe was quantified. The pressure head equals the vertical distance between the air inlet of the compact water cylinder and the top of the soil sample. The travel distance corresponds to the height of the sample. By weighing the buckets collecting water before and after each time span and recording the duration, the water flux (Q in m^3/day) can be computed. For Darcy's Law, Q must be divided by the surface area of the sample which is 20 cm^2.

$$Q = -A\, k_{sat}\, \frac{dh}{dx} \qquad (1)$$

Eq. (1) Darcy's Law (Hendriks, 2010), with discharge Q in m^3/day, surface area of soil sample A in m^2, saturated hydraulic conductivity Ksat in m/day, pressure head dh in cm and travel distance dx in cm.

The discussion of measured plot parameters was mainly focused on the attributes that were used in this study and summarized in Table 1. An elaborate description of plot construction and measurements was executed in the research of van de Lisdonk (2023). The amount of data of in-situ ksat data is relatively small as purckhauer measurements excluded measurements of ksat values.

Table 1. Attributes derived from plot measurements employed in this study

Type of measurement	Characteristic	Technique
Vegetation	Vegetation classes and description	*Photographs / field*
Soil	Profile description (soil texture, rock fragments and depth)	*Field*
Hydrology	Ksat	*UU Lab*

2.3.3 Distribution of ground measurements

Primarily to conducting fieldwork at the Meretschibach catchment. A RF model classified 5 vegetation classes (forest, shrubs, grass, pioneer and bare soil areas) by using Sentinel-2 imagery as training data (Appendix 4). Within these 5 classes, 8 plots per class had to be distributed randomly across the upper Meretschibach catchment. This was done by using random stratified sampling of locations within each class. In contrast to purckhauer measurements, the plot construction included bare soil descriptions and analyses.

All measurement locations, both plots and purckhauers, were surveyed using an Emlid Reach RS. This device is a Global Navigation Satellite System (GNSS) and is used for Real Time Kinematic (RTK) and Post Processed Kinematic (PPK) surveying and geospatial software for data collection and processing. The Emlid tracks signals from GPS, GLONASS, BeiDou, QZSS and Galileo and is centimetre-accurate. The reference station used in this research was a Continuous Operating Reference Station (CORS) installed in Leuk, Switzerland (HOH2). All locations were georeferenced by post-processing the Emlid data with the CORS.

As a result, a total of 42 plots were established and 111 purckhauer measurements were assessed. The research on plot parameters encompasses the entire upper Meretschibach catchment (van de Lisdonk, 2023). As a consequence, not all plot locations lay within the area covered by the UAV missions. Hence, 11 purckhauer data points and 19 plot data points were excluded from this research since the location of these measurements were beyond the outline of the study area. As a result, a total of 23 plots and 100 purckhauer measurements were used for statistical modelling. The distribution of plot and purckhauer data within the study area is illustrated in Figure 7.

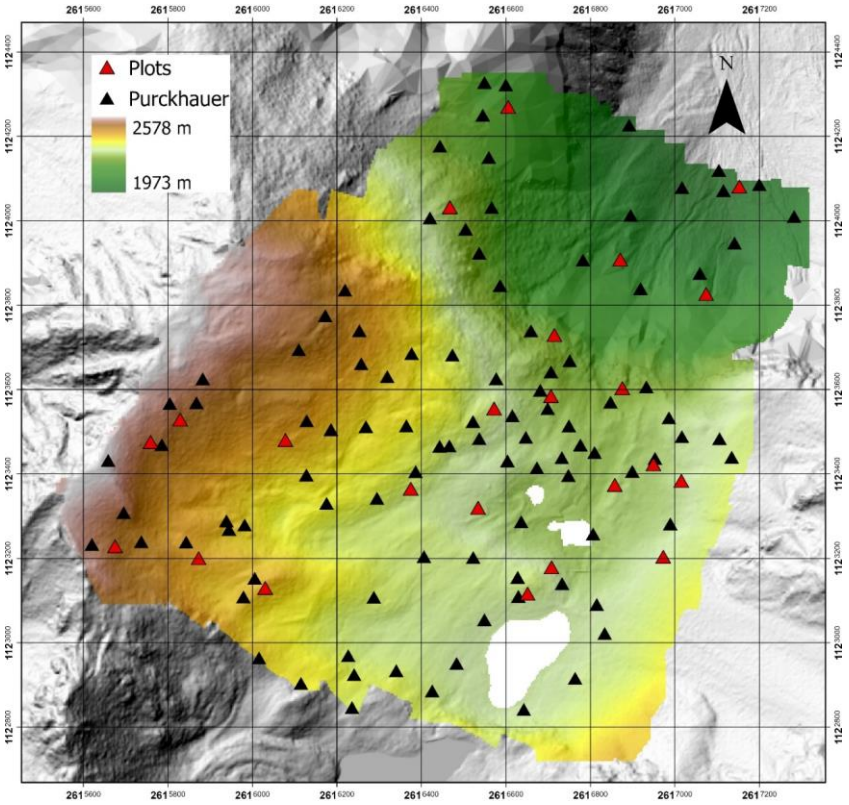

Figure 7: Spatial distribution of field measurements in boundaries of the area captured by UAV missions, on DEM elevation raster (25 x 25 cm).

2.4 Statistical Modelling

2.4.1 Random Forest model

Random Forest (RF) models were used as statistical models in this research. Random Forest creates an ensemble of decision trees, each trained on a random subset of training data, a process known as bootstrap aggregating (Ali et al., 2012). As a result, different trees were created with multiple bootstrap samples which ensures diversity among the trees. A tree initiates from the roots and is build-up of nodes and leaf nodes or terminals (Appendix 5). A random subset of training data features was considered for each tree at each node which in turn decorrelates the trees. Hence, RF models are less sensitive to outlier data and are prone to overfitting due to bootstrap aggregating (Ali et al., 2012). Each tree was trained on a subset of training data. Therefore, some sample data was not used in the RF model, also known as out-of-bag (OOB) sample data (Ishwaran et al., 2021). The OOB sample data was used for predicting accuracy of RF models and generated automatically by the randomForest() package in R.

In addition, prediction of both nominal as continuous variables could be constructed by using RF models. Furthermore, variable importance and accuracy were generated automatically for both continuous and nominal data. Random Forest (RF) modelling was considered as a promising technique to predict soil properties (Ließ et al., 2012; Pahlavan-Rad et al., 2020; Peters et al., 2007; Prasad et al., 2006). Therefore, statistical modelling was generated by Random Forest modelling in this research.

2.4.2 Random forest training data

The decision trees of the RF models were build-up of different nodes representing a random subset of training data. The training data consists of attributes derived from UAV, Sentinel-2 and Swiss ALTI3D terrain data (Table 2).

The UAV data includes high resolution ortho imagery and DEM terrain indices. Ortho imagery was already sufficient to build a reasonable model for SOC prediction (Yang et al., 2021). DEM terrain attributes as for example slope correlated most highly with surface soil attributes in research of Moore et al. (1993). In addition, it is important to consider statistical differences of pixel values within a prediction grid cell. For UAV data, pixel size was smaller than the grid cell size (Figure 8).

A gray-level co-occurance matrix (GLCM) is a statistical method used to describe spatial relations between pixels in a greyscale image. A GLCM can be used to extract various texture features from UAV imagery. This variation in image texture is expressed in GLCM mean value, variance, homogeneity, contrast, dissimilarity, entropy and second moment (Özkan et al., 2023). All features of GLCM were considered in this study as statistical operators in prediction and to analyse variable importance of each feature. Hence, gray-level co-occurance matrix (GLCM) attributes were added to the training data (Table 2).

The Sentinel-2 data includes difference in NDVI from 2019 to 2022 (for the months May, June, July and August), snow persistence and day of the year snow free (Table 2). Monthly NDVI data from 2019 to 2022 for these months could reveal patterns of growth and NDVI intensity at different elevations which could be closely correlated to vegetation patterns in the study area. Also, day of the year snow free correlates with a value for each pixel that is closely related to the start of the growing season. Snow persistence correlates with a time period for the presence of snow in the study area, indicating for example no vegetation growth during that period. Therefore, these Sentinel-2 data has been added to the training data as all attributes could be of impact on vegetation, hydrology and soil texture (Table 2).

SwissALTI3D data includes terrain attributes (Table 2). These terrain attributes were derived from SwissALTI3D as this data covers the entire Meretschibach catchment. Therefore attributes dependent on flow accumulation had to be derived from datasets that covered the entire upper Meretschibach catchment. Hence, UAV data could not be used to calculate these secondary terrain attributes as it covers just a segment of the catchment. The attributes derived from SwissALTI3D data have a direct or indirect impact on soil texture and hydrology (Bishop & Minasny, 2006; Li et al., 2020; Maier et al., 2020; Moore et al., 1993) and were hence considered as training data.

Table 2: Training data for generating decision trees of random forest models for predicting soil properties and vegetation.

Source	**Training data**
DEM (25 x 25 cm), eBee UAV missions	Mean & standard deviation: - Slope - Aspect - Elevation
Ortho (10 x 10 cm), eBee UAV missions	Bands, mean & standard deviation: - Red - Blue - Green - Re - NIR Gray-Level Co-occurrence Matrix (GLCM) - Mean - Variance - Homogeneity - Contrast - Dissimilarity - Entropy - Second moment
Sentinel-2 (10 x 10 m)	- Difference in NDVI for monthly data over 2019-2022 • May • June • July • August - Day of the Year Snow Free - Snow Persistence.
SwissALTI3D (2 x 2 m)	- Flow accumulation - Terrain Wetness Index (TWI) - Stream Power Index (SPI) - Length Slope Factor (LS) - Terrain Ruggedness Index (TRI) - Topographic position index (TPI)

2.4.3 Random Forest model prediction

The random forest model was derived from the randomForest package in R (Breiman et al., 2022). The trained RF model was applied to a regular 4 by 4 m grid contained by the UAV, Sentinel-2 and Swiss ALTI3D terrain data (Figure 8). A total of 77136 grid cells conceal the area covered by the UAV missions. As a result, 77136 grid cells were predicted by RF models for both continuous and ordinal data.

Besides, soil textural classes were assigned to three fractions of clay, silt and sand. The sum of the fractions should be equal to 100% to assign a soil textural class (Figure 6). These three fractions were predicted by three independent RF regression models. Hence, the three fractions had to be corrected to sum up to a total of 100%. This was done by scaling the percentages while preserving the relative proportions of the individual values. After this correction, soil textural classes were assigned in R based on all fractions of sand, silt and clay of the soil textural triangle of Figure 6. As a result, an indirect classified soil textural result based on RF regression model predictions (Table 3).

Table 3: Overview of field variables predicted by RF modelling

Predicted data type	Variable obtained during fieldwork	Unit
Continuous	- Sand	*%*
	- Silt	*%*
	- Clay	*%*
	o Soil textural classification (USDA)	
	- Rock cover	*%*
	- Soil depth	*cm*
	- Rock fragments	*%*
	- Ksat on surface	*m/day*
	- Ksat on 10 cm depth	*m/day*
Classified	- Soil texture	*12 classes*
	- Vegetation	*4 classes*

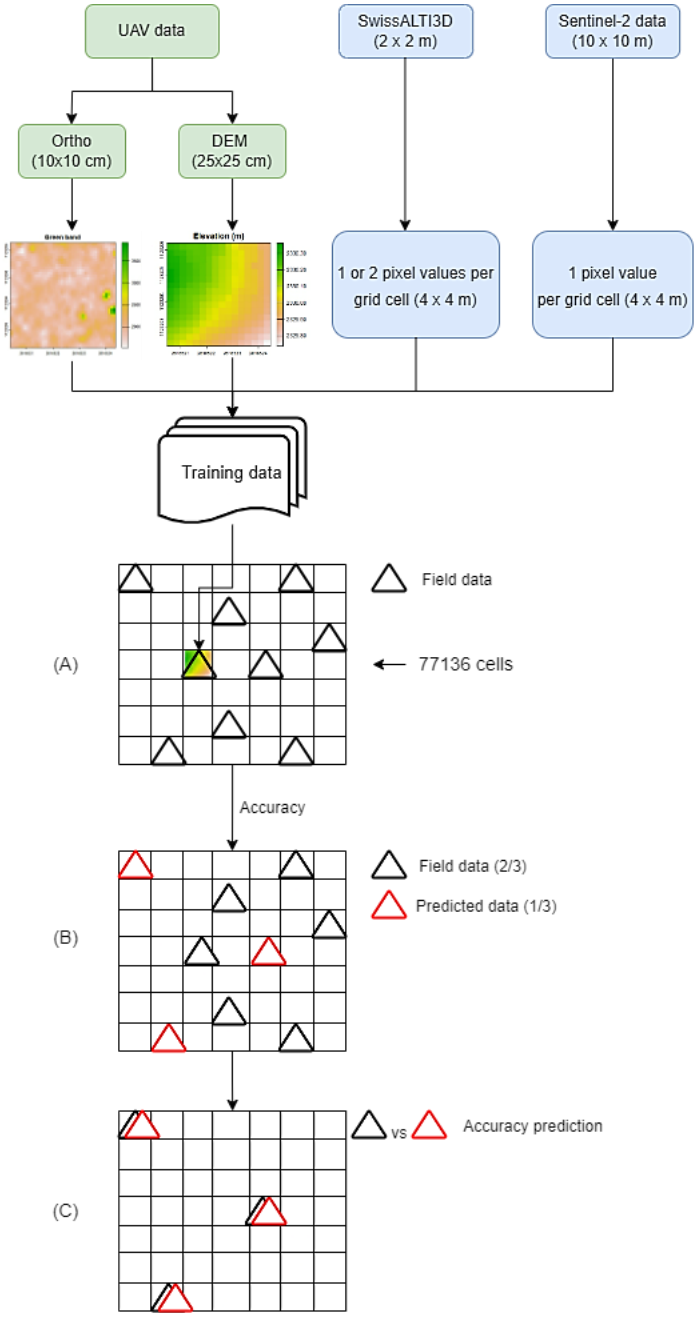

Figure 8: Flowchart delineating the steps for predicting parameters on Meretschibach catchment scale. Left vertical segment of the chart is comprised of yellow boxes that describe the sequential stages of the process, while the right segment offers a visual representation of the methods.

2.5 UNCERTAINTY PREDICTION IN DIFFERENT MODELS

2.5.1 Variable importance (VIMP) of RF models

Variable importance (VIMP) is a measure that quantifies the contribution of each feature to the accuracy of the model. The accuracy was measured on the out-of-bag (OOB) instances before and after permuting the values of a specific variable. The VIMP was based on the decrease in model accuracy when the values of a particular variable were randomly permuted (Ishwaran et al., 2021). Hence, a high decrease in accuracy indicated a more important variable. Thus, variables with higher importance values were of greater impact on the overall predictive performance of the model.

The RF models were predicted by different variables. Some variables may be more important compared to other prediction variables to predict a certain parameter. The findings from Fox et al. (2017) study propose that variable predictors with moderate to low importance could be incorporated into the model with minimal impact on the predicted probabilities. It will be investigated whether the prediction accuracy could be enhanced by creating different scenarios. After determination of VIMP in scenario 1, two other scenarios were tested to check accuracy differences for prediction of continuous data.

- Scenario 1 includes all training data for RF model prediction.
- Scenario 2 includes the top 10 most important variables of scenario 1 as training data for RF model prediction.
- Scenario 3 excludes the top 10 least important variables of scenario 1 as training data for RF model prediction.

2.5.2 Uncertainty prediction for random forest classification

For validation of *classification* by a random forest model, a confusion matrix is generated by the randomforest() package, which describes the accuracy using a portion of the data that is not used for prediction also known as out-of-bag (OOB) samples.

$$(OOB)\ Misclassification\ rate\ = \frac{FP+FN}{TP+TN+FP+FN} \qquad (4)$$

In Eq. (4) (Maria Navin & Pankaja, 2016), TP: true positive, TN: true negative, FP = false positive and FN = false negative and Table 3 reveals the condition for each variable.

Table 4: Confusion matrix (Maria Navin & Pankaja, 2016)

	Predicted: No	**Predicted: Yes**
Actual: No	TN	FP
Actual: Yes	FN	TP

In addition, the examination of other metrics to assess the performance of the RF models include the (OOB) Area Under Curve (AUC) and the (OOB) Brier score (Brier, 1950; Holmes et al., 2021; Ishwaran et al., 2021), since the randomforest() package in R incorporates the computation of these values.

The AUC measured the area under the Receiver Operating Characteristic (ROC) curve and is independent of threshold selection for classification and a useful method for evaluating the classification accuracy of a model (Fawcett, 2006). An example of a ROC curve was attached for clarification of an area under a ROC curve (Appendix 6). The AUC of a classifier is equivalent to the

probability that a classifier, when assigning classes, will assign a higher probability to a randomly chosen positive instance than to a randomly chosen negative instance (Fawcett, 2006).

The positive instance corresponded to the class of interest and the negative instance correlates with the classes that should not be assigned to this instance. Therefore, a higher AUC indicates that the classifier is more likely to assign higher predicted probabilities to classes of interest than to the wrong class. An AUC of 0.5 indicates classifying at random whereas 1.0 indicates perfect classification. The higher the AUC the better the classifier (Holmes et al., 2021).

Furthermore, the Brier score is a useful metric for assessing the probabilistic predictions. However, in comparison to the AUC, the Brier score did not consider the specific decision threshold for classification.

$$(OOB)\ Brier\ score = \frac{1}{N}\sum_{i=1}^{N}(pi - ai)^2 \qquad (5)$$

In Eq. (5) N: number of instances, p: the predicted probability for instance i and a: is the actual outcome for instance i (Brier, 1950). The Brier Score is a measure of accuracy of probabilistic predictions ranging from 0 to 1. A perfect classifier has a Brier Score of 0.

2.5.3 Uncertainty prediction for random forest regression

The accuracy of predicted RF regression models was determined by calculating the out-of-bag (OOB) coefficient of determination (R^2) and the Root Mean Square Error (RMSE) for RF regression. A very low coefficient of determination can be observed in a completely linear model (RMSE close to 1), and conversely, a high R^2 can occur in the presence of a non-linear model (RMSE close to 0) (Chicco et al., 2021).

$$(OOB)\ R^2 = 1 - \frac{\sum_{i=1}^{n}(Fi-Pi)^2}{\sum_{i=1}^{n}(Fi-\bar{F})^2} \qquad (2)$$

In Eq. (2), Fi: the value measured in the field, Pi: the predicted value from the RF model, $\bar{F}$: the measured average of field values and n: the number of observations. The coefficient of determination can be understood as the fraction of the variance in the dependent variable that can be predicted by the independent variables (Chicco et al., 2021). The coefficient of determination is optimal for value 1 and could mathematically have a negative infinite value representing the worst coefficient. Hence, values close to 0 suggest poor predictive performance. Negative values suggest that the model's prediction was worse than the mean of the response variable. Therefore, negative values suggest that the model was not capturing the patterns in data effectively.

Moreover, to further evaluate the models performance an additional validation technique was performed. The RMSE was calculated separately from the generated (OOB) R-squared by the randomforest() package. Then, two third of the field data was used to train the model. As a result, the remaining one third was predicted by this RF model. The one third that was not used for prediction, could now be cross-validated with the predicted one third to calculate the RMSE.

$$RMSE = \sqrt{\frac{1}{n}\sum_{i=1}^{n}(Fi - Pi)^2} \qquad (3)$$

In Eq. (3), Fi: the value measured in the field, Pi: the predicted value from the RF model and n = the number of observations. To obtain more stable results and better estimations for the RMSE the same calculation was repeated a 100 times for each dataset. The RMSE has value 0 if the model fits the data perfectly and could mathematically have an infinite positive value for the worst fit of the model.

3 RESULTS

3.1 IN-SITU GROUND MEASUREMENTS

The soil textural classes and vegetation types classified by purckhauer measurements and establishment of plots in the study area were plotted in Figure 9. Soil textures were determined in 10 different soil texture classes (Figure 9a). The most dominant soil texture classes acquired in the high alpine study area comprised high sand fractions like sandy loam, sandy clay loam and loamy sand (75% of soil textural findings). The vegetation classes in the study area consist of 1 bare soil area, 67 shrubs, 28 grass and 19 forest classes (Figure 9b).

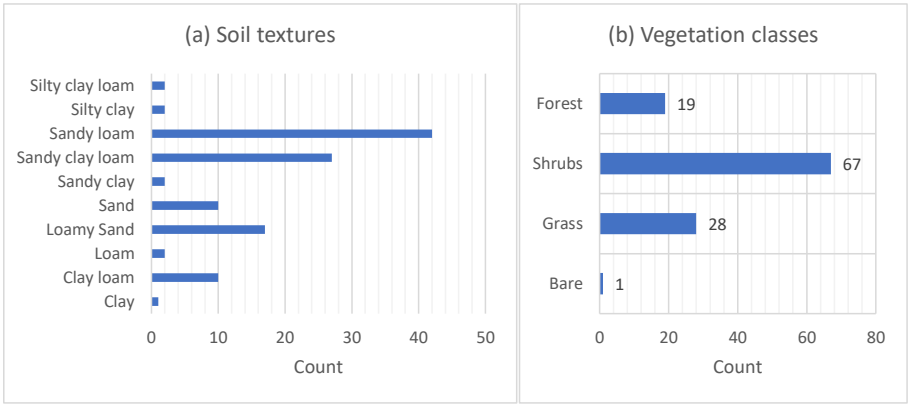

Figure 9: The amount of different soil textural classes (a) and vegetation classes (b) determined by in-situ field measurements.

The relation between vegetation and soil texture was plotted in Figure 10. Forest areas correlate with sandy soil textures (sandy loam and sandy clay loam, sand and loamy sand). Sandy clay and clay were only measured at locations where shrubs were the dominant species. Silty clay loam, silty clay, sandy loam, sandy clay loam, sand, loamy sand, loam and clay loam were all determined at both grass and shrubs.

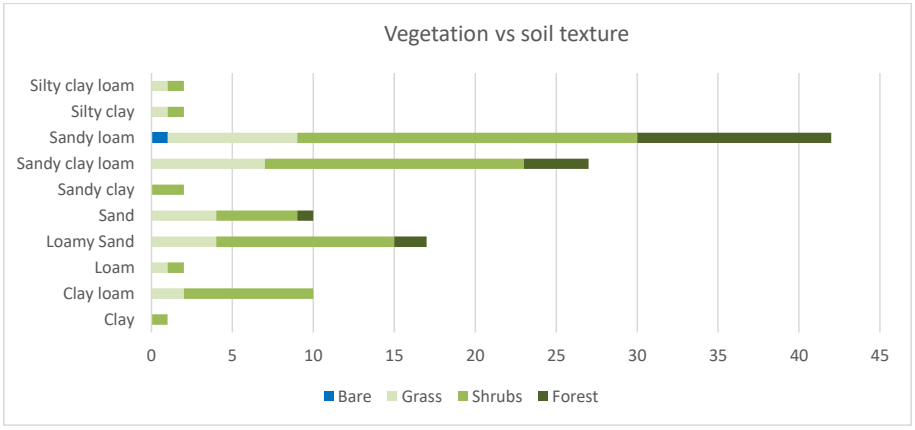

Figure 10: A stacked bar plot visualizing the relation between soil textural classes and vegetation classes.

3.1.1 Relations between soil textures and statistical variables

Figure 11 illustrates soil textural relations between important parameters derived from the field data. Figure 11a is a boxplot of soil texture versus elevation in meters. Loam and silty clay are only classified at lower elevations (roughly <2300 m) compared to the other soil textural classes.

The soil texture-**slope** relation is plotted in Figure 11b. Loamy sand, sandy loam and sandy clay loam were determined on the steepest slopes > 45° of the study area. Sand was measured at moderate slopes ranging from 10° till approximately 35°. Sandy clay, clay, clay loam, silty clay and silty clay loam were determined at slopes smaller than 25°. Silty clay and silty clay loam were both determined at flattest slopes < 15°.

Figure 11c shows the relation between the soil texture and the **TWI**. The average TWI value for clay loam, loam, loamy sand, sand, sandy clay, sandy clay loam, sandy loam and silty clay were all between 2 and 6. For silty clay and clay the TWI was measured at ~6.5. Sitly clay loam had the highest TWI value > 12 and the lower TWI value of silty clay loam was ~5.0.

Figure 11d shows the relation between **soil depth** and soil texture. The sandy soil textures (sand, sandy loam, sandy clay loam, loamy sand) were present at locations with soil depths deeper than 60 cm. Clay, clay loam, loam, sandy clay, silty clay and silty clay loam all had a less deeper soil varying from 10 cm depth till 55 cm depth.

Figure 11e shows the soil texture versus the **rock cover** percentage at the surface. Sandy loam includes the highest rock cover percentage which represents a bare soil area > 85%. Clay was also determined at a location with a high rock cover percentage of 60%. Sand, sandy clay loam and sandy loam all vary from 0% up to 60% rock cover. Clay loam and loamy sand range from 0% to 40%. Loam, sandy clay and silty clay loam were rock cover percentages only determined below 10%.

Figure 11f visualizes the **rock fragments** versus the soil texture. The percentages of rock fragments were relatively high (some values higher than 40%) for loamy sand, sandy clay, sandy clay loam and sandy loam. Loam, silty clay and silty clay loam almost excluded rock fragments in the soil as rock fragment percentages were < 5%.

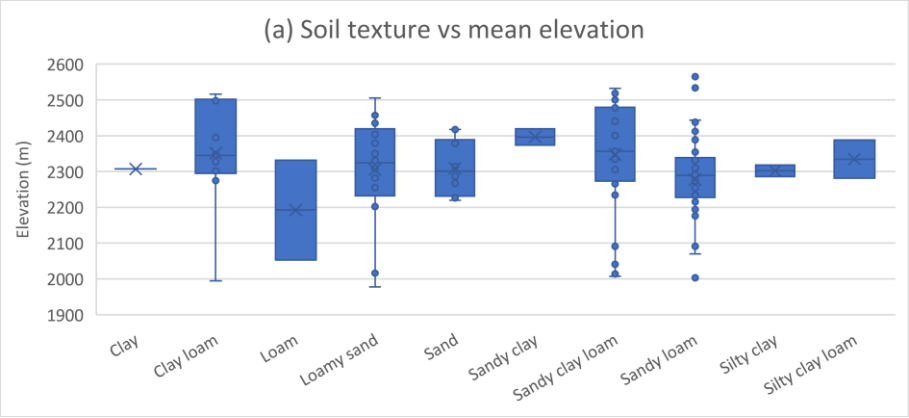
(a) Soil texture vs mean elevation
Elevation (m)
2600
2500
2400
2300
2200
2100
2000
1900
Clay
Clay loam
Loam
Loamy sand
Sand
Sandy clay
Sandy clay loam
Sandy loam
Silty clay
Silty clay loam

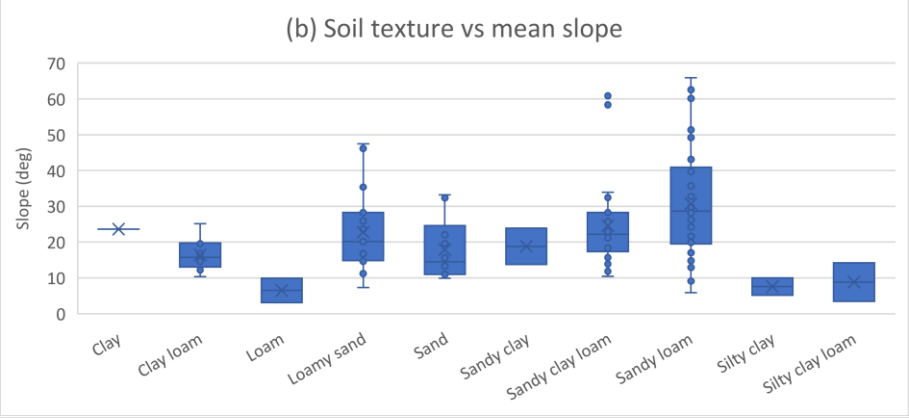
(b) Soil texture vs mean slope
Slope (deg)
70
60
50
40
30
20
10
0
Clay
Clay loam
Loam
Loamy sand
Sand
Sandy clay
Sandy clay loam
Sandy loam
Silty clay
Silty clay loam

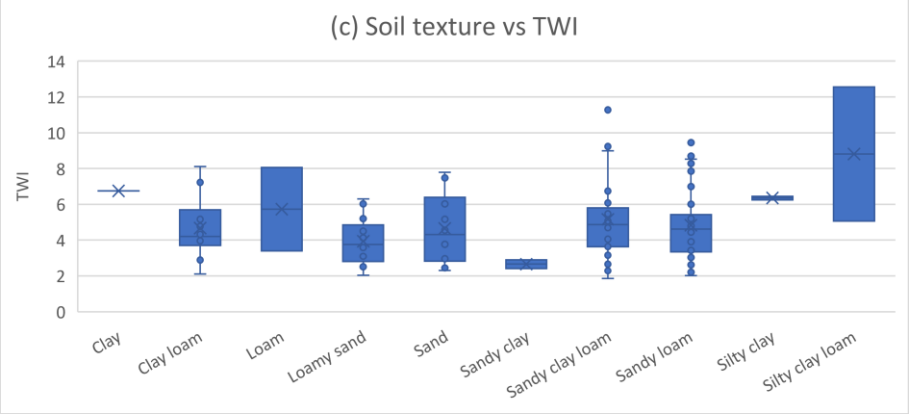
(c) Soil texture vs TWI
TWI
14
12
10
8
6
4
2
0
Clay
Clay loam
Loam
Loamy sand
Sand
Sandy clay
Sandy clay loam
Sandy loam
Silty clay
Silty clay loam

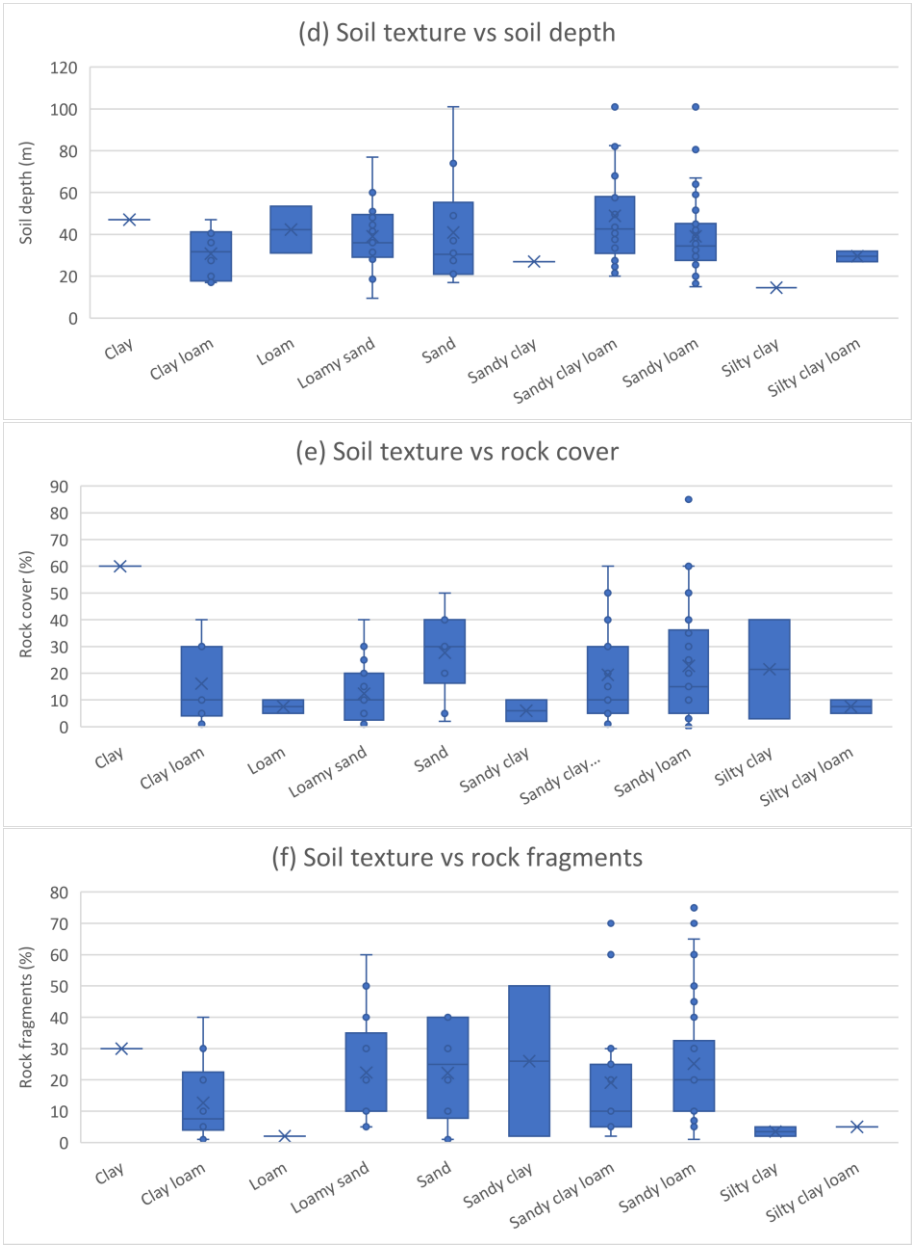

Figure 11: (a) shows the elevation in meters related to the soil texture determined in field, (b) shows mean slope vs soil textural class and (c) shows calculated TWI vs soil textural class. (a), (b) and (c) are all related to UAV derived parameters. (d) shows the soil textural class versus the soil depth (m), (e) soil texture vs soil depth and (f) soil texture vs rock fragments. (d), (e) and (f) are all parameters measured or estimated in the field.

3.1.2 Relations between vegetation and statistical variables

Figure 12a shows a boxplot of vegetation type vs **elevation**. The plot showed that the forest class is located on lower elevations (< 2300 m). Different shrubs were growing on all elevation levels in boundaries of this study area (2100 m till 2550 m) with a few outliers below 2100 m. The alpine grasslands were situated at higher elevations (>2200 m till ~2520 m). The bare class was measured at an elevation of 2388 m.

Figure 12b reveals the steepness of the **slopes** compared to the vegetation type. The slope was relatively high for the forest classes (32° < gradient < 65°). Shrubs were growing on slopes varying from 10° degrees to 40°. The slope was relatively low (30° < gradient < 4°) for locations dominated by grass. The bare class had a slope of ~21°.

Figure 12c shows the boxplot of vegetation type versus **topographic wetness index (TWI**), the TWI values for grass, shrubs and forest show similar spreads (2 < TWI < 9) with forest reaching the highest TWI values up to ~11. All classes had the median TWI value between 4 and 6. The bare plot had a TWI of 4.8.

Figure 12d reveals the boxplot of vegetation versus **soil depth**. Forests had the deepest soils according to the box plot ranging from 20 cm up to a minimal depth of 101 cm (max. length purckhauer). Whereas grass and shrubs had smaller soil depths ranging from ~15 cm to ~68 cm for grass and ~10 cm to ~60 cm for shrubs. The bare class had a soil depth of 39 cm.

Figure 12e shows the **rock cover** percentage for each vegetation type. As expected, the bare class rock cover percentage was 85%. For forest the rock cover percentage was relatively low ranging from 0% to 20%. The grass and shrubs had a similar range in rock cover percentages from 0% to 60%. Grass had the highest median (25%), shrubs had a moderate median (15%) and forest had the lowest median (5%).

Figure 12f shows the boxplot relation between **rock fragments** in the soil versus the vegetation type. For shrubs and forests the measured rock fragments percentages were quite similar (0% < Rock fragments < 60 %). For grass the rock fragments were ranging from 0% to 70%. The rock fragments in the soil determined at the bare plot was equal to 10%.

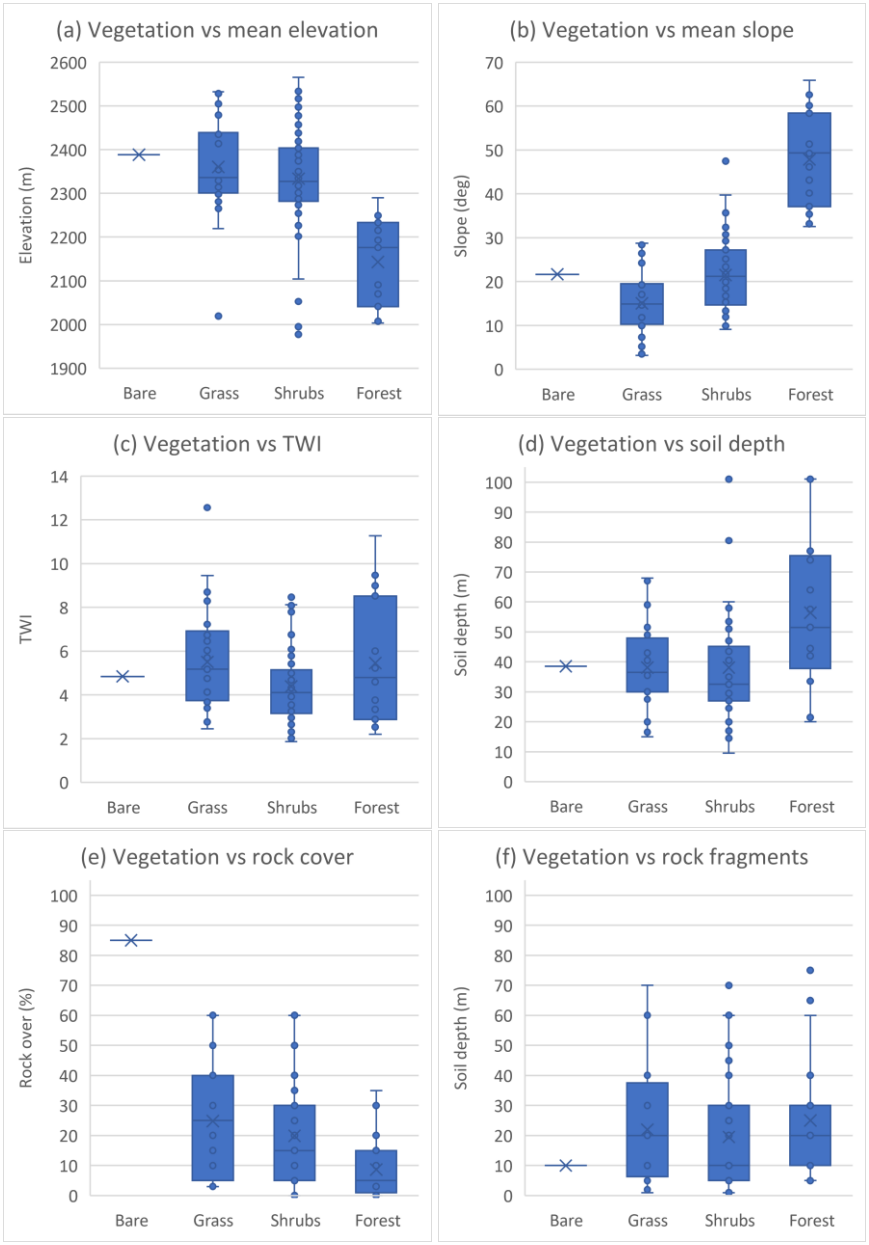

Figure 12: a, b and c represent boxplots of vegetation type versus UAV derived parameters whereas d, e and f boxplots of vegetation type versus in situ measurements

3.2 RF MODEL PREDICTION MAPS

The RF classification model and RF regression model predictions were visualized in different maps. All results of RF models were based on scenario 1 and therefore including all training data in the RF models. Water bodies were excluded as primarily land parameters were predicted. Therefore, all maps include 3 white areas in the south eastern corner of the UAV flight area. These areas were assigned NoData values as they represent the Unter Meretschisee and the two small lakes near the hydropower company. All maps shown in section 3.2 contain a hill shade layer (2 x 2 m) derived from SwissALTI3D data. The hill shade layer enhances visual appeal of the maps and provides valuable information to better understand the topography, including slopes and elevations of the landscape.

3.2.1 Maps classified using Random Forest

The soil texture and vegetation were predicted using RF models for classification prediction. Both maps were visualized in Figure 13.

The vegetation map (Figure 13a) represents 4 different classes: bare soil, grass, shrubs and forest. The bare soil class is scarcely present and only evident in the southwestern part on the talus slopes. The grass was classified mainly in the southeastern, the relatively higher part of the study area. The shrub class was the most dominant class predicted and covered a large part of the area. The forest class covered the northern lower part of the area. Despite a few predicted forest classes south of the Unterer Märetschisee.

The RF classification model for soil texture based the prediction on the soil textures determined in the field (Figure 9a). Figure 13b shows the predicted distribution of soil textures throughout the study area. The predicted classes that were highly present in the soil texture maps are sandy loam, sandy clay loam, loamy sand and sand. The predicted classes that were barely present are clay, clay loam, loam and silty clay.

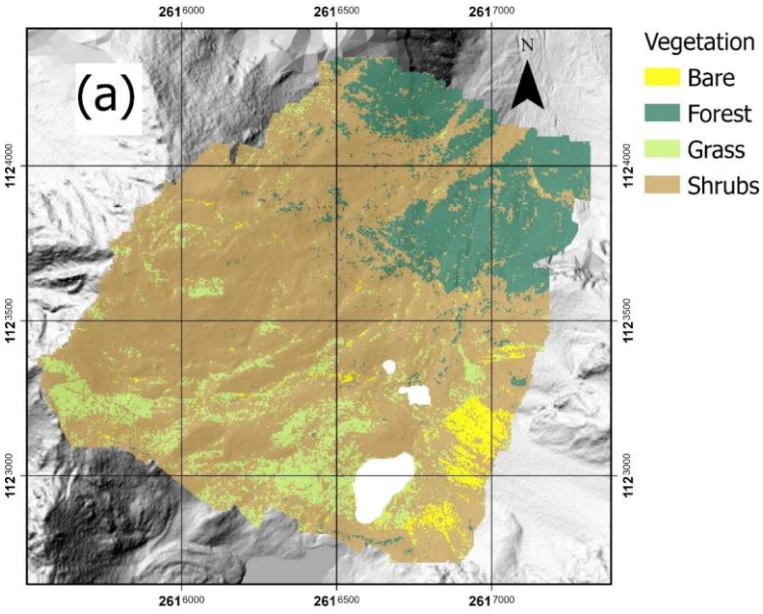

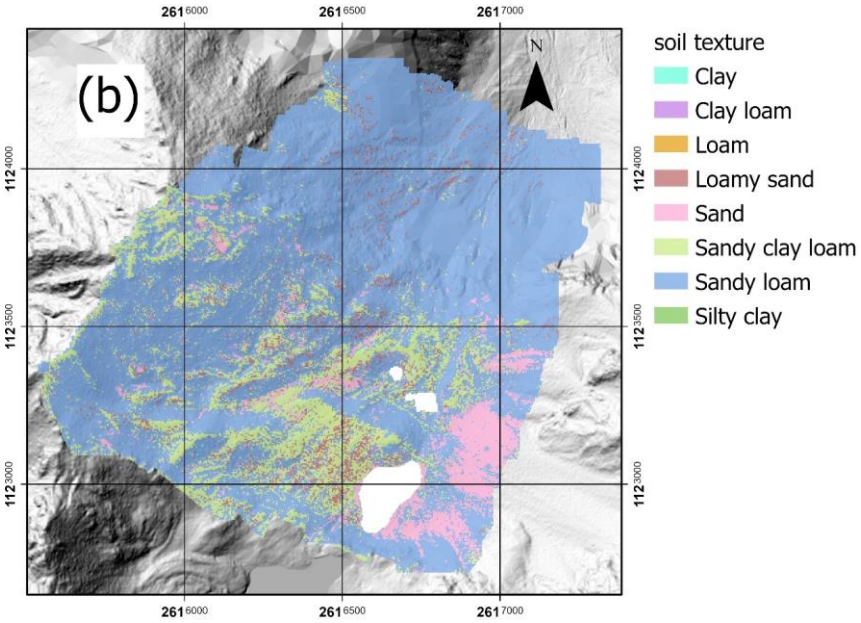

Figure 13: RF classification model predicted vegetation map (a) and soil texture map (b).

3.2.2 Regression maps generated by using Random Forest

The first RF regression models were based on the soil textural field data. Figure 14 includes sand, silt and clay percentages and a soil textural classification.

Figure 14a shows the sand percentages predicted throughout the study area. The predicted sand percentages range from 34% to 75%. Hence, based on the sand percentages soil textures with higher sand percentages (>75%) like sand or lower sand percentages (<34%) like silt, silty clay and silty clay loam were excluded in the RF regression model prediction (Figure 6). Sand percentages were high in the northern part of the study area and relatively low near the three lakes in the south-eastern part.

Figure 14b shows the silt percentages predicted in the study area. The predicted silt percentages range from 10% to 40%. Likewise, soil textures with higher silt percentages (>40%) and lower silt percentages (<10%) were not predicted. Therefore, silt loam was also not predicted in addition to the soil textural classes already excluded by sand percentage prediction (Figure 6). The silt percentages were relatively high near the three lakes in the south-eastern part and lower values were present across the entire study area (Figure 14b). Moderate silt percentages were mainly visual at the talus slopes in the south-eastern corner of the study area.

Figure 14c shows the clay percentages predicted across the study area. The predicted clay percentages range from 11% up to 31%. Similarly, soil textural classes with higher clay percentages (> 31%) and lower clay percentages (<11%) were not predicted. Thus, based on the USDA textural triangle (Figure 6), sandy clay and clay were not predicted as soil textural classes in addition to the other excluded classes. The clay percentages were relatively low in the northern part, moderate in the south-western part and highest near the three lakes in the south-eastern part of the study area.

Figure 14d shows a classified soil textural map. The combination of sand, silt and clay percentages represent a certain soil texture. This classification was based on the USDA textural triangle (Figure 6). The most dominant soil texture in the study area was predicted as sandy loam and sandy clay loam (Figure 14d). In addition, loam and clay loam were predicted near the Unter Märetschisee. Loamy sand was mainly predicted in the northern forestry part of the study area.

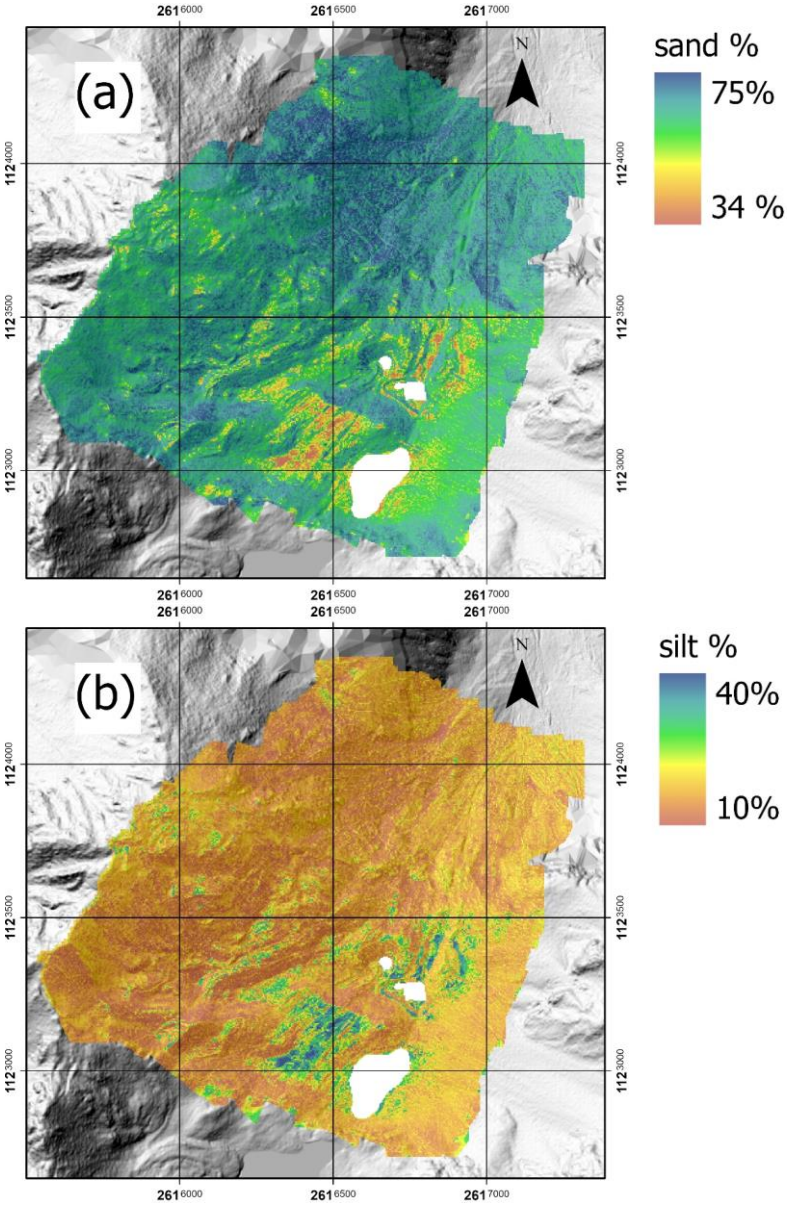

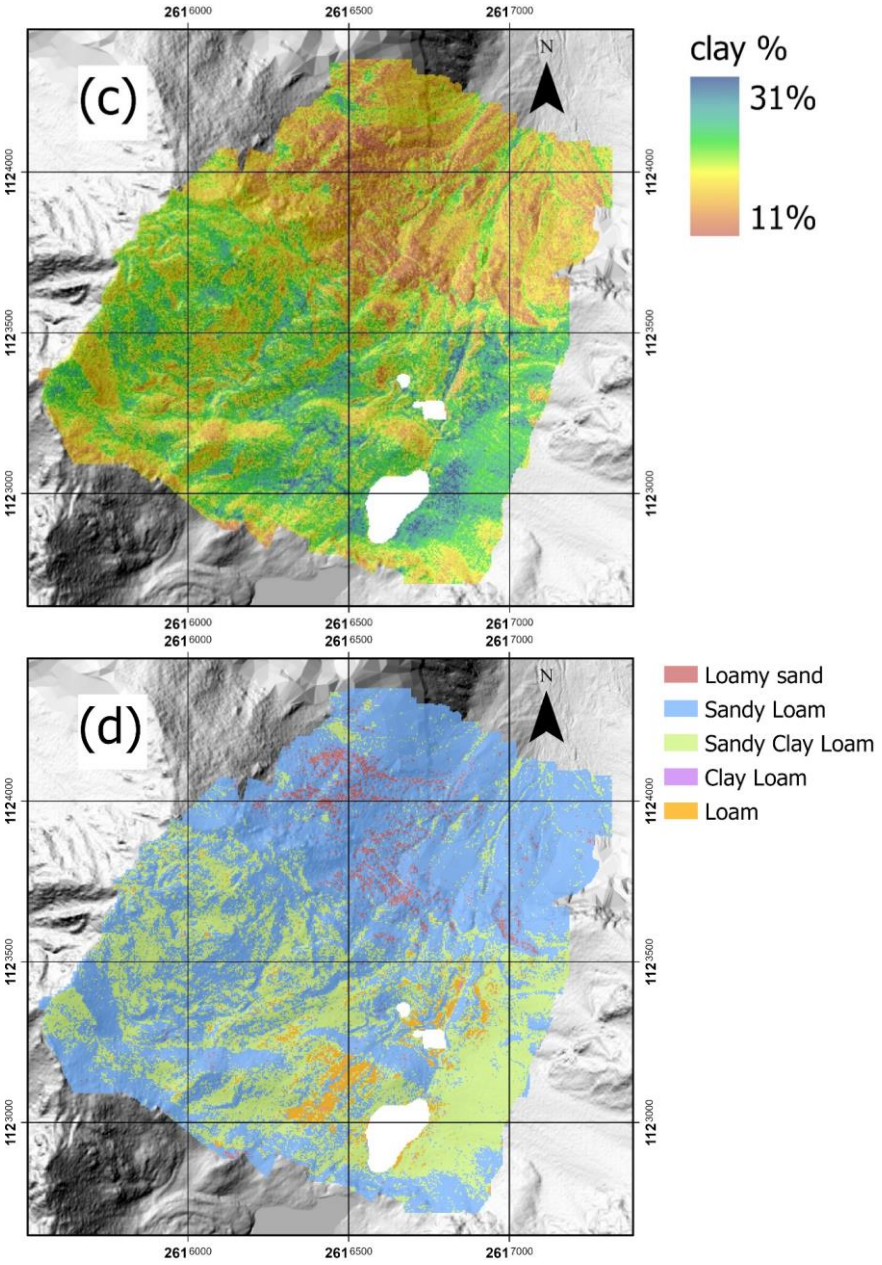

*Figure 14: (a) sand, (b) silt and (c) clay show predicted soil textural percentages for the study area. Map (d) shows the classified soil texture by combining map (a), (b) and (c). Map (d) was derived from the USDA textural triangle (*Soil Survey Manual, 2017*).*

Likewise, three predicted maps were shown in Figure 15 displaying rock cover percentage, soil depth and percentage of rock fragments in soil.

Figure 15a shows the rock cover percentages were higher in the southern part of the study area and lower in the northern part of the study area. Rock cover percentage ranges from 3% to 75%. Highest values were visible on talus slopes in the south-eastern part. Also, high rock cover percentages were visible in segments in the upper south-western part. Rocks and vegetated areas could be easily identified on the high resolution ortho photo (Figure 4). Similar patterns visible in the ortho photo and the rock cover percentage map were noticeable throughout the study area. Figure 15a also shows that the rock cover percentage were mostly visible in the green colour (3% – 15%) or red colour (63% – 75%).

Figure 15b reveals a map of the predicted soil depth in the study area. The predicted soil depth ranges from 25 cm till 70 cm. The soil depth was deepest is the northern part which correlates with forested areas. The southern part west of the Upper Märetschisee reveals the shallowest soil depths where grass is mostly predicted.

Figure 15c shows a predicted map of rock fragments in the soil. The predicted rock fragment percentages in soil range from 8% till 44%. Higher rock fragments were predicted on talus slopes, on higher rock cover percentages and in the forest. Therefore, in contrast with rock cover percentages, rock fragments were found in deeper soils and where vegetation is classified as forest.

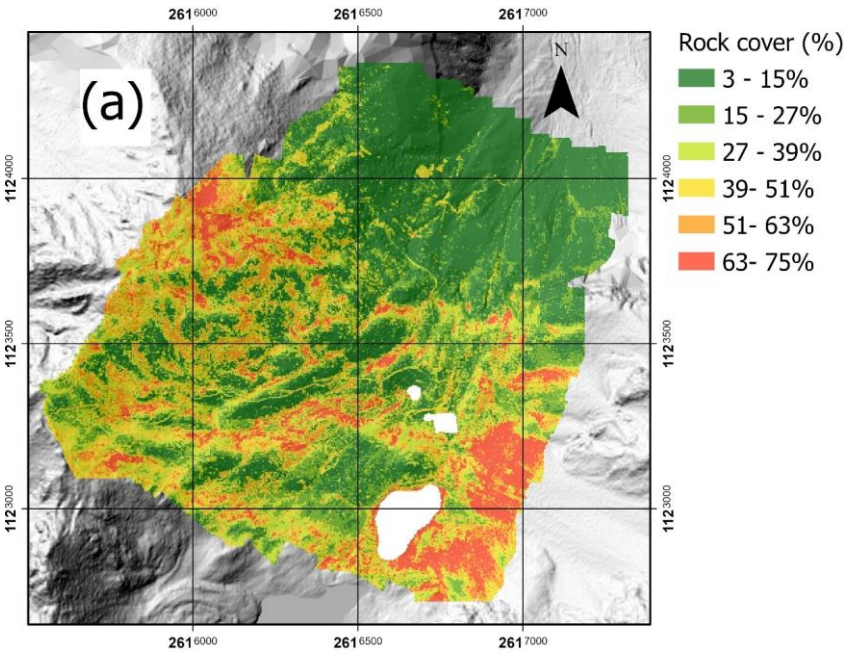

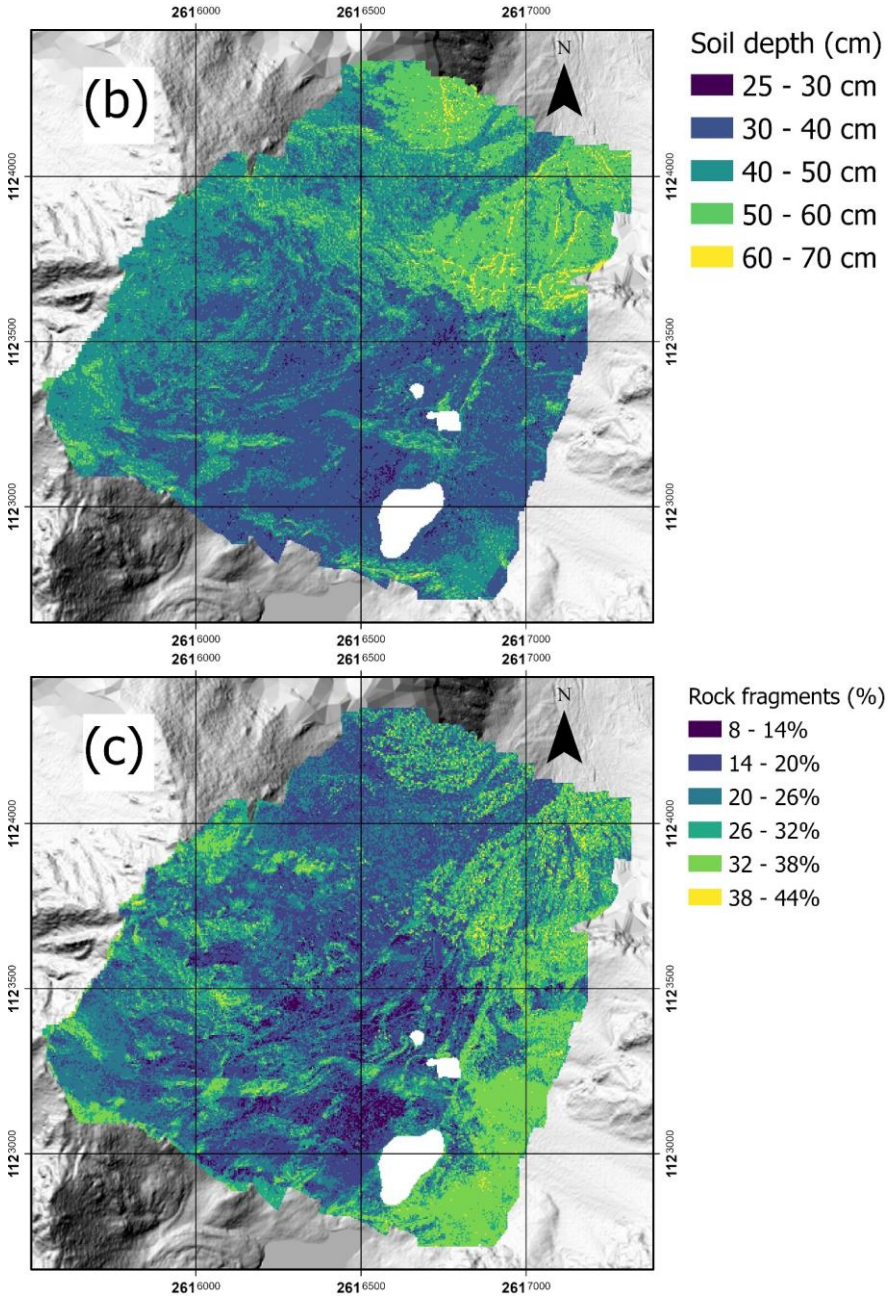

Figure 15: Map (a) shows rock cover prediction by the random forest model. Map (b) shows soil depth and map (c) contains the percentage of rock fragments in the soil.

RF model prediction of ksat

The resulting ksat maps were displayed in Figure 16. Figure 16a shows the ksat surface values ranging from 14 m/day up to 54 m/day. The ksat surface values were higher at locations with high rock cover percentages and at the northern part of the study area were forest was located. Figure 16b shows the ksat on 10 cm revealing a wider range from 4 m/day up to 92 m/day. The ksat on 10 cm map shows higher values on the talus slopes in the southeastern corner of the study area and higher values in the northern part.

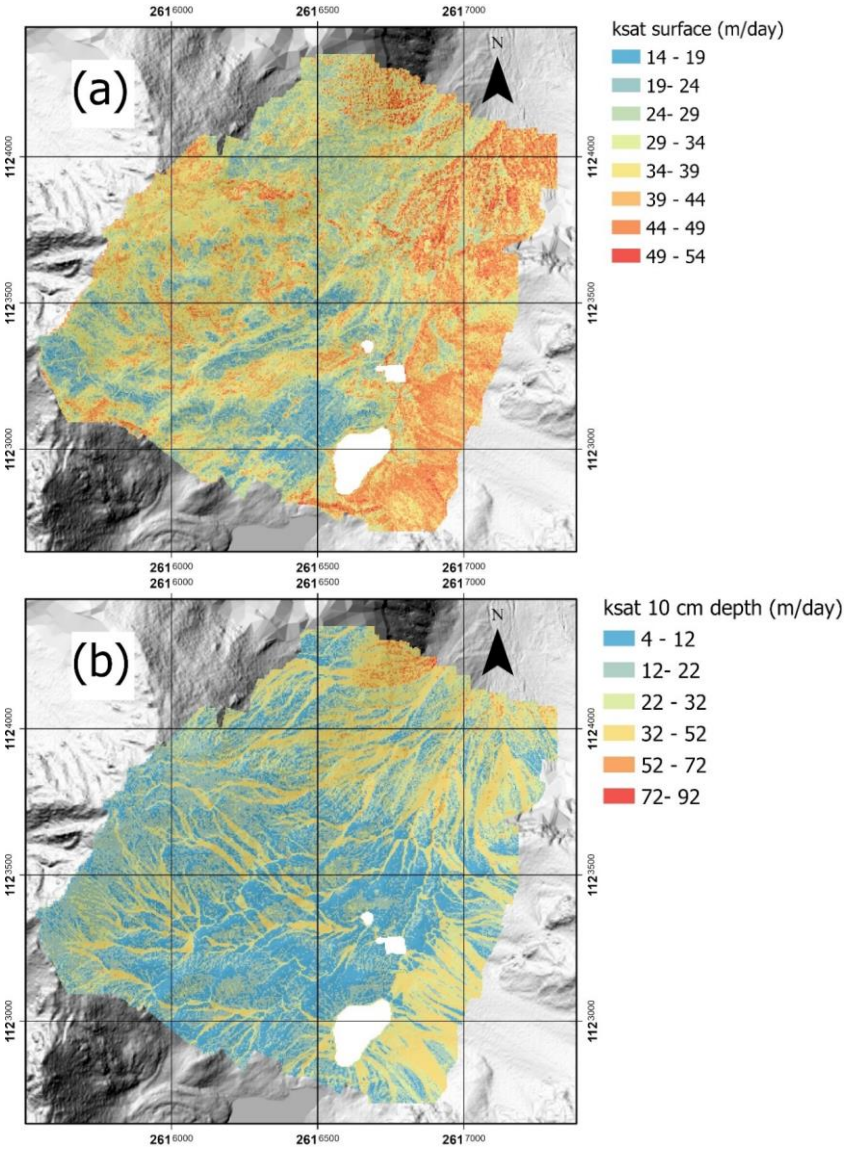

Figure 16: Maps of predicted values for saturated hydraulic conductivity (ksat) on surface (a) and on 10 cm depth (b).

3.3 Random Forest variable importance and model accuracy

3.3.1 Variable importance of RF models

The variable importance (VIMP) is a measure that quantifies the contribution of each feature to the accuracy of the RF model. The top 10 most important variables of scenario 1 were plotted for the RF regression models (Appendix 8). As a result, the most important variables for scenario 1 were summarized below.

VIMP for RF **classification** models:

- Prediction of soil textural classes: *LSF* and *SPI,* feature derived from SWISSALTI 3D data
    - In addition, elevation, slope and green spectral bands from UAV data.
- Prediction of vegetation: *slope* and *elevation,* derived from UAV data
    - Spectral bands, day of the year snow free, difference in NDVI of July, June, August, May. Features from UAV data and Sentinel-2 data.

VIMP for RF **regression** models**:**

- *Sand* and *silt* prediction: mean slope and the standard deviation in elevation, features from UAV data.
- *Clay* prediction: terrain ruggedness index (TRI) and the Length Slope factor (LSF), features from SWISSALTI 3D data.
    - The important variables for *sand, silt* and *clay* prediction were closely related to erosional variables. Features of the SWISSALTI 3D data like TRI, LSF, TWI and SPI were all important for prediction of soil textural percentages (Appendix 8).
- *Rock cover* percentage: the mean values of the blue band and the difference in NDVI for the month June, features from UAV and Sentinel-2 data respectively.
    - The important variables for *rock cover* percentage prediction were dominated by visual band features (Blue, Green, Red, NIR) from the UAV data. In addition, snow persistence was also an important predictor for mapping rock cover percentage of the study area.
- *Soil depth* prediction: TPI and the standard deviation in elevation, features from the UAV and SWISSALTI 3D data.
    - The prediction of *soil depth* was dominantly predicted by Topographic Position Index (TPI), elevation, snow persistence (A3) and day of the year snow free. Additionally, the spectral bands (Blue, Green and NIR) and the mean slope were important features that contributed to the accuracy of the model.
- *Rock fragment* percentage in soil: NIR mean and standard deviation in Re band, features from UAV data.
    - The important variables for predicting *rock fragment* percentages were the mean of the near infrared (Nir) band, the green spectral band and the standard deviation of the red edge (Re). In addition, aspect parameters and snow persistence were also important features.

In further analyses of accuracies of the different RF regression models different scenarios were analysed. The RF regression model prediction of scenario 2 included the features present in the top 10 of most important variables of scenario 1 (Appendix 8) and excludes all other features as training data. The RF regression model prediction of scenario 3 excluded the top 10 least important variables of scenario 1 (Appendix 9).

3.3.2 RF classification model performance

The accuracy of both soil texture and vegetation was determined using a confusion matrix. The misclassification rate of soil texture was 61.1% and the vegetation map had a misclassification rate of 19.5%. The correlating confusing matrix for vegetation and soil texture was shown in Figure 17 and Appendix 13 respectively.

The bare soil areas were incorrectly classified as 100% was of the bare classes was misclassified. Only one forest class was misclassified resulting in a prediction accuracy of approximately 95% for forest. 15 grass classes were wrongly predicted resulting in a accuracy of 46% correct predicted grass classes. The shrubs had a high percentage of approximately 95% of classes that were accurately predicted. A misclassification rate of 19.5% indicated that 99 classes were correctly predicted and only 24 classes were incorrectly predicted.

```
Confusion matrix:
          predicted
observed Bare Forest Grass Shrubs class.error
  Bare      0      0     1      3      1.0000
  Forest    0     18     0      1      0.0526
  Grass     1      0    13     14      0.5357
  Shrubs    1      2     1     68      0.0556

     (OOB) Misclassification rate: 0.195122
```

Figure 17: Confusion matrix of observed vegetation classes vs predicted vegetation classes

The confusion matrix of soil texture (Appendix 13) revealed highest percentage of correctly classified sandy loam classes of approximately 79%. Followed by sand with 40% correctly classified and sandy clay loam had 24% correctly classified. revealed *misclassification* rate of 100% for clay, clay loam, loam, loamy sand, sandy clay, silty clay and silty clay loam.

The errors of both soil texture and vegetation were summarized in Table 5. The Brier scores of both vegetation and soil texture were relatively low indicating low probabilistic predictions. The AUC for vegetation is 0.931 and for soil texture just above 0.5. Therefore, AUC for vegetation indicates almost perfect classification (1.0) and for soil texture the (OOB) AUC reveals that classifying was almost done at random (0.5).

The RF model for classification of vegetation had the highest overall accuracy. A low brier score close to 0. The closer the AUC is to 1.0, the better the classifier (Holmes et al., 2021) and the RF vegetation model shows an AUC value of 0.931 indicating almost perfect classification. In addition, the misclassification rate of vegetation is only 19.5% indicating that only 24 out of 123 classes where incorrectly predicted from the RF model. Therefore, the vegetation classification prediction was superior to the RF model prediction of soil textural classes.

Table 5: The Out Of Bag (OOB) accuracies for the RF classification models. Requested performance error = Misclassification rate

Classification	(OOB) Brier score	(OOB) AUC	(OOB) Requested performance error
Vegetation	0.0705	0.931	0.195
Soil texture	0.0769	0.537	0.611

3.3.3 RF regression model performance

The RF regression model performance was assessed using both the root mean square error (RMSE) and the out-of-bag (OOB) coefficient of determination (R^2). Table 4 summarizes the accuracy values of the different RF regression models and different scenarios.

The RF regression model for predicting the rock cover percentage has the highest R^2 of 0.57. All other RF models show low R^2 values (< 1.0). The accuracies were also determined for scenario 2 and scenario 3 (Appendix 11). Both scenarios show minor variations in R^2 outputs compared to scenario 1. Scenario 2 showed slightly more variations compared to scenario 3. The (OOB) R^2 of rock cover increased from 0.57 to 0.60 for scenario 2.

The predicted values versus the observed values were plotted in Figure 18. The red line signifies the one-to-one line, where points would align if all predicted parameters were accurately estimated. All RF regression models show RMSE values larger than or equal to 10. The observed and predicted values of the sand percentage show the smallest dispersion with the red line (RMSE = 1) indicating perfect prediction (Figure 18). It is evident that the various regression models pose distinct performance accuracy. All RMSE were derived from different parameters and therefore different scales (Figure 18). Normalization of the RMSE was necessary to facilitate the comparison of these RMSE values. This was done by dividing the RMSE by the range between the maximum and the minimum observed values obtained from Figure 18 and Appendix 7 (for ksat).

The Normalized RMSE (NRMSE) revealed that sand percentage had the most accurate value of 0.13 followed by 0.17 of the prediction of rock cover percentage. The NRMSE for ksat revealed the highest error indicating the least accurate results.

The predicted ksat values in the RF model were derived from a limited dataset comprising only 20 field parameters. The variable importance exhibited inconsistencies while re-evaluating the model. Consequently, the filtering of important variables for scenario 2 and 3 was inconsistent and as a result excluded from this research, noted as x in Appendix 10.

Table 6: Random Forest (RF) regression model accuracies for scenario 1 which included all input parameters.

RF Models	Data	Train	Predict	**RMSE**	**NRMSE**	**(OOB) R^2**
Sand (%)	115	77	38	10.0	0.13	-0.035
Silt (%)	115	77	38	11.2	0.25	0.011
Clay (%)	115	77	38	11.5	0.29	0.010
Rock cover (%)	123	82	41	14.8	0.17	0.57
Rock fragments (%)	121	80	41	17.8	0.25	-0.102
Soil depth (cm)	100	67	33	20.6	0.29	0.054
UU lab:						
Ksat_surface (m/day)	19	15	4	29.6	0.37	-0.078
Ksat_10 (m/day)	17	12	5	9.6	0.34	0.016

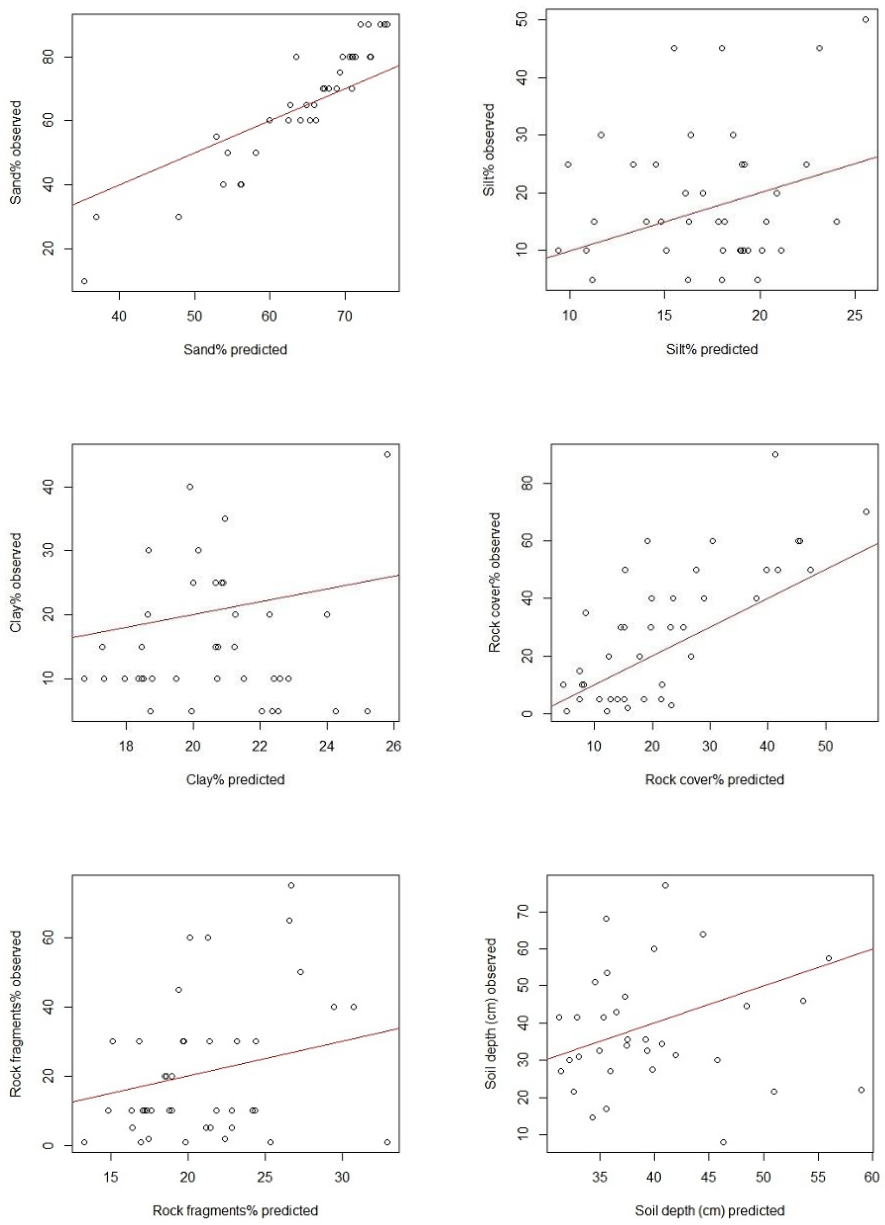

Figure 18: Predicted vs observed values plotted for continuous data. Red line shows the one-to-one line for the best fit (observed = predicted).

4 DISCUSSION

4.1 SPATIAL DISTRIBUTION OF SOIL PROPERTIES AND TERRAIN CHARACTERISTICS

The study area in the Meretschibach was comprised of different vegetation and soil textural classes. The dominant vegetational class determined in the study area was shrubs and the dominantly present soil textural class was sandy loam. In line with the expectations, soil textures were relatively coarse in this study area. Overall, the dominant soil textural classes (75% of total classes determined) had a relatively high sand percentage e.g. sandy loam, sandy clay loam and loamy sand.

The alpine soils in the study area were considered as young soils as grain size was relatively large. The grain size distribution depends on the parent material, with more recently weathered material being coarser and alpine soils being generally younger (Körner, 2021). This is primarily caused by the comminution of soil particles through the process of congelifraction (Oztas & Fayetorbay, 2003).

Various sandy soil textures were measured on the steepest slopes of the study area. In the Alps, soil patterns are primarily influenced by microtopography, particularly in areas above the timberline (Baruck et al., 2016). The soil texture on hill slopes are generally coarser due to erosion and transportation processes, whereas valleys and plains typically exhibit finer soil texture because of sediment deposition (Dharumarajan & Hegde, 2022). The concept of shallow subsurface flow (Bauer, 2010), results in a higher sand/clay ratio as altitude increases. This phenomenon occurs on steeps slopes and with overland flow distance to the channel network, where finer particles were transported downslope directly beneath the soil surface. The forest class revealed the steepest slopes, lowest rock cover percentages and the deepest soils. Hagedorn et al. (2019) suggested that vegetation below the timberline have a thick organic layer and deeper root zones at lower elevations. Thus, forest growing on steeper slopes had developed strong and extensive root systems in stable soils and therefore maintain a secure foothold.

Coarser soils with higher sand fractions have a higher porosity. Moreover, the measured sandy soil textures did contain a higher amount of rock fragments compared to silty soils, which enhances the porosity. The growth of vegetation and the release of root exudates advance chemical weathering, involving the leaching and breakdown of primary minerals and the formation of secondary minerals like clay minerals (Maier et al., 2020). Hence, fine substrates like clay could accumulate through the soil to deeper levels of the soil (Körner, 2021). Therefore, it is expected that in areas with deeper soils a more clayey soil texture could be determined on a deeper level.

In contrast, flatter slopes correlated with finer soil particles and less deeper soils in this study area. Silty soils were only determined on flatter gradients of the study area. Furthermore, grass was also primarily developed on less steeper slopes and had a high rock cover percentage. Therefore, soil textures measured on flatter parts of the study area correlated with finer soil particles and less deeper soils. The cohesive clay minerals could stabilize soil particles (Lado et al., 2004). In addition, the soils with higher silt and clay fractions also revealed low rock fragment percentages and shallower soil depth.

Vegetation cover shifted from forest on lowest elevations to shrubs and grass on higher elevations. The vegetation cover is highest in forestry areas (as it included trees, shrubs and grass) and lowest for bare soil areas. Ksat was expected to decrease with higher elevation and less vegetation, as vegetation cover is expected to increase microporosity and thus increase ksat (Maier et al., 2020). As a result, the ksat was expected to increase in the northern part of the study area since this segment is covered by forest, which it did as seen in Figure 16a. The predicted ksat surface value were also high for high rock

cover percentages (Figure 15a). The talus slopes have a high rock cover percentage describing bare soil areas. Areas covered by rocks have a complex hydrology. The presence of rock debris covering soils has a positive impact on moisture retention in the root zone of alpine vegetation, this is achieved by interrupting the capillary continuity of soil moisture (Körner, 2021). Large rocks may create macropores that enhance water movement and drainage, which potentially increase ksat. Conversely, densely packed rock debris may hinder water movement and reduce ksat.

In conclusion, high surface ksat values on areas correlated with relatively high rock cover percentage and forestry areas. In contrast, soils with lower microporosity will decrease ksat. In the research of Maier et al. (2020), soil texture had a bigger impact on ksat than vegetation growth. he arrangement of soil particles, involving both aggregation and capillary water retention, is predominantly influenced by the interaction between clay minerals and organic matter (Velde & Meunier, 2008). Organic matter and clay play a dominant role in cation exchange and retention, providing favourable conditions for plant growth (Egli & Mirabella, 2021). Therefore, using soil texture as input for ksat predictions could increase the performance of such a prediction model. Furthermore, the amount of input data on ksat was minor as 19 locations on surface and 15 locations on 10 cm depth included average ksat measurements. The prediction of ksat based on RF models can potentially be more accurate if more ksat measurements were conducted in this study area. In addition, Furthermore, a different method could be applied to predict these values such as the mean value method. The mean value method could be useful when there is limited amount of data available (Ließ et al., 2012). Nevertheless, the average ksat values that are known for these locations could potentially be included RF models as input for predicting other parameters.

4.2 Random Forest classification model performance

Field data and UAV imagery were applied to estimate soil properties and vegetation by using Random Forest (RF) classification models. Both soil textural prediction and vegetation prediction had a low (OOB) Brier score correlating with low probabilistic predictions (Brier, 1950).

The RF classification model for prediction of vegetation classes was superior in prediction performance. The results showed that 81.5% of the vegetation classes was correctly classified. In addition, the (OOB) AUC of vegetation was close to 1 representing almost perfect classification. The accuracy of predicting shrubs and forests was the highest. Previous studies revealed an overall accuracy rate of 65% for vegetation map data (Zhou et al., 2016).

The RF classification model for prediction of soil texture was less accurate. The results suggested that 39.9% of the soil textural classes was correctly classified. The sandy loam class was most accurately predicted. Also, soil texture classification had an (OOB) AUC close to 0.5 which corresponded to random classification. Previous studies revealed an overall accuracy rate of 50-65% for prediction of soil textural classes at different depths (Dharumarajan & Hegde, 2022).

4.3 Random Forest regression model performance

The RF regression model performed best for prediction of rock cover percentages in the study area. The (OOB) R-squared represents the variance of the dataset. The (OOB) R-squared was determined with out-of-bag (observed) data that were excluded from the prediction. The (OOB) R-squared value is a statistical measure that represents the proportion of variance between the predicted values and the observed values. The (OOB) R-Squared ranges from 0 to 1, with 1 indicating a perfect fit (Chicco et al., 2021). The (OOB) R-squared of the *rock cover* percentage prediction was highest for all scenarios, with a moderate R-squared of 0.57. Indicating that the RF regression model for rock cover prediction

performance revealed the largest proportion of variance that is explained by independent variables, in contrast to the other models. Hence, this suggests that this RF model was moderate in capturing and predicting the variability in the data. The model performance for rock cover prediction showed minor improvements of higher (OOB) R-squared values (up to 0.60) for scenario 2 and 3.

The (OOB) R-squared for silt, clay, soil depth and ksat at 10 cm depth was low ($R^2 < 0.1$). A significant proportion of the variability in the dependent variable was not explained. The RF model may not be capturing important factors that were of influence on the dependent variable. All model prediction models show small improvements from scenario 1 to 2 (Table 4), for example R-squared of silt prediction changed from 0.011 to 0.075.

The RF regression model predictions of sand, rock fragments in soil and hydraulic conductivity (ksat) on surface all show negative coefficients of determination. A negative R-squared indicates that the model's predictions were worse than a simple horizontal line which represents the mean of the dependent variable (Chicco et al., 2021). Therefore, the RF model failed to capture the patterns or trends in the data, and its predictions are less accurate than a basic model that merely predicts the mean.

In addition, the Root Mean Square Error (RMSE) was calculated to gain a comprehensive understanding of the model's performance. The RF regression model predictions all showed RMSE values larger than 9.0. As the range of RMSE stretches from 0 to +∞ as upper bound, it is hard to quantify the quality of such a result (Chicco et al., 2021). The plot of the observed sand values showed the best visual fit compared to the other plots. However, the RMSE of sand percentage was higher than the RMSE of ksat on 10 cm depth. The scale of each plot is different and therefore the RMSE values could not be compared. Normalization was necessary to compare the accuracies of the RF regression models.

The models performance was considered good for NRMSE values between 0.10 and 0.20, fair for values between 0.20 and 0.30, and deemed poor for values greater than 0.30 (Ge et al., 2021). As a result, the models performance for prediction of sand and rock cover percentage was considered good. The models performance of for prediction of silt, clay, rock fragments and soil depth was considered fair and the NRMSE of ksat prediction were largest (> 0.30) indicating poor model simulation.

4.3 VARIABLE IMPORTANCE OF RANDOM FOREST MODELS

4.4.1 Variable importance of soil texture

The mean slope and the standard deviation in elevation were the most important variables for predicting sand and silt percentages. For clay percentages the most important variables were Terrain Ruggedness Index (TRI) and the Length-Slope Factor (LSF). In addition, erosional features (e.g. TRI, LSF, TWI and SPI) were also important for the accuracy of soil texture predictions. These results were in line with previous studies that revealed that terrain indices were of major importance for soil textural predictions (Dharumarajan & Hegde, 2022; Jena et al., 2023; Kaya et al., 2022; Moore et al., 1993).

The relation between slope and soil textures revealed that sandy soil textures were dominant on steeper slopes. Length-Slope Factor (LSF) is a measure of the sediment transport capacity of overland flow (Moore & Burch, 1986). The LSF was higher for sand, sandy loam and sandy clay and suggested that these soil textures had a higher soil erosional risk potential (Appendix 11). This indicated that these soil textural classes contained steeper and/or longer slopes. Furthermore, higher sand percentages correlated with higher SPI values (Appendix 11). SPI was an important feature for

predicting sand, silt and clay percentages. SPI is a parameter to quantify power of flowing water, low SPI indicating less power. In the research of Jena et al. (2023) coarser soil fractions indicated higher SPI values. Moreover, The TRI values were larger for sandy textures compared to the other soil textures (Appendix 11). Terrain Ruggedness Index (TRI) offered a comprehensive assessment of the overall ruggedness of the landscape by considering elevation variations over a larger area. Higher TRI values correlate with more rugged terrain and lower TRI values suggest smoother or flatter terrain.

In contrary, higher clay percentages were observed and predicted on flatter areas in this study area. TWI indicates the spatial distribution of soil moisture, high TWI values indicate wetter conditions. Flatter areas often correlate with higher TWI values, consequently TWI has the potential to serve as an indicator for augmentation of clay content within a flood plain (Jena et al., 2023).

4.4.2 Variable importance for rock cover & vegetation prediction

The most important variables for rock cover prediction and vegetation were closely related. The most important variables included spectral bands, difference in NDVI for month June over 2019-2022 and snow persistence. The most important variables were in line with the expectations, as rocks were clearly visible due to the reflection of different wavelengths compared to vegetation and can therefore be visually distinguished. Also, a high NDVI value indicates a greater abundance of healthy vegetation. NDVI indices ranging from -1 to 0 represent non-vegetated surfaces (Xu et al., 2012). The difference in NDVI for the month June over the period of 2019-2022 could be of great impact due to timing and potentially a peak of vegetation growth and therefore showing largest variation in NDVI in June to differentiate between bare rock surfaces and vegetational cover compared to the importance of NDVI for the other months.

Another important variable for rock cover prediction was the snow persistence variable. Therefore snow persistence value separates between bare soil and vegetated area. In Appendix 12 the snow persistence input map is included. The map visualizes higher snow persistence values on higher elevations and especially in the southeastern corner of the map the values are high. Talus slopes were present in the south eastern corner of the study area.

Timing and duration of snowpacks influence initial growth of different vegetation species. The soil is cooled during the growing period with increasing canopy height of shrubs and trees, as indicated by (Körner, 2021). Conversely, during winter periods, the canopy height warms the soil in winter by advancing the accumulation of an insulating snow cover (Myers-Smith & Hik, 2017). Early snowmelt may stimulate vegetation development and growth. Therefore, rock cover percentage and vegetation will be influenced by changes in the timing or duration of snowpack development. The timing and duration impacts different facets of the soil-vegetation systems in regions experiencing temporary snow cover (Edwards et al., 2007).

Other studies also revealed that elevation and temperature were the most important variables for vegetation prediction (Zhou et al., 2016). As alpine catchments can be subdivided into different vegetation belts on different elevations, it was expected that elevation would be of greater impact on prediction of vegetation.

4.4.3 Variable importance for prediction of soil depth

The prediction of soil depth throughout the study area, the most important variables were TPI, elevation, snow persistence and day of the year snow free. This could be coupled to the vegetation belts. Larger vegetation growth indicate increasing soil depths (Hagedorn et al., 2019). As vegetation decreases in size for higher elevations, soil depth potentially decreases as well. The observed data also revealed deeper soils for the forest class and for lower elevations. Therefore, elevation and the Topographic Position Index (TPI) features were of major importance for estimating soil depth.

The Topographic position index indicated whether a pixel is higher or lower than its surrounding pixels. However, due to the resolution (2 x 2 m), the values of TPI could be less representative for microtopographic variations within a grid cell with a size of 4 x 4 m. The TPI could have been derived from the UAV imagery (25 x 25 cm) if the malfunction did not occur which could increase interpretation of microtopographic differences within a prediction grid cell and potentially be better for predicting variables.

4.5 FUTURE STUDY MODEL PREDICTIONS

The accuracies of multiple RF model in this research for different parameters were diverse. Other statistical methods could be tested since not all RF model predictions showed accurate results. Likewise, several studies have compared the linear regression methods and machine learning techniques to see which model is superior in spatial soil properties prediction. Farooq et al. (2022) found that RF models performed better than RK (and OK) for SOC mapping in Himalayan region of Kashmir. In contrast, Veronesi & Schillaci (2019) demonstrate that the OK model performs slightly better as predictor for topsoil organic carbon than the RF model. For fields with high sampling densities kriging and regression kriging are promising compared to random forest models to map SOM (Pouladi et al., 2019). Takoutsing & Heuvelink (2022) state that no universal model works best and therefore RK or RF could perform better for a specific case. Thus, the optimal technique depends on spatial distribution and size of soil samples data, terrain attributes, elevation, climate conditions and vegetation. Hence, multiple methods have to be tested to find the optimal soil prediction mapping result for a specific study site. Therefore, it could be tested whether the Random Forest method is superior for this specific study area by testing other models for this specific site.

5 CONCLUSION

This research used remote sensing and statistical modelling to potentially upscale vegetation and soil properties to an alpine catchment scale. The remotely sensed data consisted of high resolution UAV data and satellite data. The application of field data and UAV imagery for estimation of soil properties was done by using Random Forest (RF) models as statistical models. The randomForest() package in R was used to build numerous RF models. Both RF regression models and RF classification models applied training data obtained from remotely sensed data in combination with field data to upscale field data to the size of the study area. The spatial distribution of soil properties and vegetation in the Meretschibach catchment and its link to terrain characteristics was summarized below.

- Soil textural predictions resulted in maps with sandy loam as dominant soil textural class. The dominant soil textures (75% of total), both measured and predicted, established high sand fractions (> 50% sand). In summary, sandy soil textures were determined on relatively steep slopes and were determined at deeper soils. Whereas silty soils were only determined on flatter parts of the study area. Sandy soil textures did contain a higher amount of rock fragments compared to silty soils. Sandy soil textures were relatively covered by a higher amount of rocks on the surface compared to silty soils.
- Vegetation predictions resulted in maps with shrubs as dominant vegetation class. Shrubs were found at a wide range of elevations, had a moderate slope, a maximum soil depth of 60 cm and were moderately covered by rocks. Grass was determined at the higher elevations, less steeper slopes and grass had the highest median of rock cover percentage. Shrubs and grass correlated with almost all soil textural classes present in this alpine catchment. In contrary, soil textures determined in the forest were all sandy soils. Forest was found at the lower elevations with steepest slopes, lowest rock cover percentages and the deepest soil depth.

Multiple field parameters were predicted by RF models. The accuracy of the RF model was studied. The vegetation map showed the highest accuracy for prediction of classes, with a misclassification rate of 0.195. The RF regression model for rock cover prediction showed the highest (OOB) R-squared (0.57) capturing a moderate proportion of the variance in combination with a low NRMSE (0.17) reflecting good RF model performance. The regression models for sand, silt, clay, rock fragments, soil depth and both ksat outputs failed to capture important factors influencing the dependent variable (OOB R-squared < 0.10). However, sand percentage reflected good model performance by determination of NRMSE. The NRMSE of silt, clay, rock fragments and soil depth predictions reflected fair model performance. At last, the NRMSE of ksat predictions reflected poor model performance.

In general, the RF model predictions were better for larger data quantities compared to predictions with lower data availability (*ksat values*). However, future studies could potentially involve ksat values for plot locations to increase the potential of predicting other variables. Random Forest (RF) was suggested as most suitable for this research, though other methods could still be tested to see whether another method is superior for upscaling by statistical modelling.

At last, the most important prediction variables were identified. The variable importance of soil texture classes and sand, silt and clay percentages was dominated by variables like slope, elevation and secondary terrain attributes. The erosional indices were important variables for predicting soil parameters as they are of great influence on soil textural composition. The variable importance of rock cover percentages and vegetation classes was dominated by spectral bands, NDVI, snow cover,

elevation and day of the year snow free. Distinguishing between vegetation and rock cover can already be done visually as they both contain very different reflectance values.

This research could be used as a set-up on conducting parameter prediction based on field work measurements in alpine catchments. In addition, UAV imagery derived from eBee X show high potential for accurate mapping of vegetation and rock cover percentages. The soil textural classes could be used as indication of soil composition in the Meretschibach catchment. The maps created in this research could be useful for spatial analysis of the plot composition and catchment behaviour. As microtopography is of major importance for soil texture analysis in alpine catchments, future studies could perform research on microtopography in the Meretschibach catchment to potentially improve soil texture data and understand the local developments at the plots.

6 ACKNOWLEDGEMENTS

I would like to thank my supervisors Philip Kraaijenbrink and W. Immerzeel for the support throughout my entire MSc Thesis process. Gratitude is extended to P. Kraaijenbrink for invaluable assistance throughout this methodology. P. Kraaijenbrink planned and conducted the UAV flight missions and managed preprocessing and postprocessing of the UAV data for model implementation. Also, P. Kraaijenbrink constructed model examples for regression and classification RF model that I used for further analysis. I am grateful to have learned the programming language of RStudio and to adapt and create models, plots and maps by using this program. Furthermore, due to the consistency of meetings with my supervisor the process of my MSc Thesis went smoothly.

Also, I would like to thank PhD student: Esther Brakkee and MSc student: Dick van de Lisdonk for conducting three weeks of fieldwork in the Alps and for performing Lab measurements at Utrecht University. In addition, J. Eichel helped during the first week of fieldwork with determination of plant species and advice on high alpine field work since she is conducting similar research in the valley next to the Meretschibach catchment, the Turtmann Glacial catchment. At last, I would like to thank the University of Utrecht for the opportunity to do fieldwork in the Swiss Alps.

7 REFERENCES

Ali, J., Khan, R., Ahmad, N., & Maqsood, I. (2012). *Random Forests and Decision Trees*. *9*(5).

Anderson, J. R. (1976). *A Land Use and Land Cover Classification System for Use with Remote Sensor Data*. U.S. Government Printing Office.

Baruck, J., Nestroy, O., Sartori, G., Baize, D., Traidl, R., Vrščaj, B., Bräm, E., Gruber, F. E., Heinrich, K., & Geitner, C. (2016). Soil classification and mapping in the Alps: The current state and future challenges. *Geoderma*, *264*, 312–331. https://doi.org/10.1016/j.geoderma.2015.08.005

Bauer, F. (2010). *Water flow paths in soils of an undisturbed and landslide affected mature montane rainforest in South Ecuador*.

Beniston, M. (2012). Impacts of climatic change on water and associated economic activities in the Swiss Alps. *Journal of Hydrology*, *412–413*, 291–296. https://doi.org/10.1016/j.jhydrol.2010.06.046

Bishop, T. F. A., & Minasny, B. (2006). Environmental Soil-Landscape Modeling: Geographic Information Technologies and Pedometrics. *Mathematical Geology*, *38*(7), 901–902. https://doi.org/10.1007/s11004-006-9054-8

Breiman, L., Cutler, A., Liaw, A., & Wiener, M. (2022). *Breiman and Cutler's Random Forests for Classification and Regression*.

Brier, G. W. (1950). *VERIFICATION OF FORECASTSEXPRESSEDINTERMS*.

Chicco, D., Warrens, M. J., & Jurman, G. (2021). The coefficient of determination R-squared is more informative than SMAPE, MAE, MAPE, MSE and RMSE in regression analysis evaluation. *PeerJ Computer Science*, *7*, e623. https://doi.org/10.7717/peerj-cs.623

Choler, P., Bayle, A., Carlson, B. Z., Randin, C., Filippa, G., & Cremonese, E. (2021). The tempo of greening in the European Alps: Spatial variations on a common theme. *Global Change Biology*, *27*(21), 5614–5628. https://doi.org/10.1111/gcb.15820

Dharumarajan, S., & Hegde, R. (2022). Digital mapping of soil texture classes using Random Forest classification algorithm. *Soil Use and Management*, *38*(1), 135–149. https://doi.org/10.1111/sum.12668

eBee X mapping drone—Drones. (n.d.). AgEagle Aerial Systems Inc. Retrieved 7 November 2023, from https://ageagle.com/drones/ebee-x/

Edwards, A. C., Scalenghe, R., & Freppaz, M. (2007). Changes in the seasonal snow cover of alpine regions and its effect on soil processes: A review. *Quaternary International*, *162–163*, 172–181. https://doi.org/10.1016/j.quaint.2006.10.027

Egli, M., & Mirabella, A. (2021). The Origin and Formation of Clay Minerals in Alpine Soils. In *Hydrogeology, Chemical Weathering, and Soil Formation* (pp. 121–137). American Geophysical Union (AGU). https://doi.org/10.1002/9781119563952.ch6

Farooq, I., Bangroo, S. A., Bashir, O., Shah, T. I., Malik, A. A., Iqbal, A. M., Mahdi, S. S., Wani, O. A., Nazir, N., & Biswas, A. (2022). Comparison of Random Forest and Kriging Models for Soil Organic Carbon Mapping in the Himalayan Region of Kashmir. *Land*, *11*(12), Article 12. https://doi.org/10.3390/land11122180

Fawcett, T. (2006). An introduction to ROC analysis. *Pattern Recognition Letters*, *27*(8), 861–874. https://doi.org/10.1016/j.patrec.2005.10.010

Filippa, G., Cremonese, E., Galvagno, M., Isabellon, M., Bayle, A., Choler, P., Carlson, B. Z., Gabellani, S., Morra di Cella, U., & Migliavacca, M. (2019). Climatic Drivers of Greening Trends in the Alps. *Remote Sensing*, *11*(21), Article 21. https://doi.org/10.3390/rs11212527

Fox, E. W., Hill, R. A., Leibowitz, S. G., Olsen, A. R., Thornbrugh, D. J., & Weber, M. H. (2017). Assessing the accuracy and stability of variable selection methods for random forest modeling in ecology. *Environmental Monitoring and Assessment*, *189*(7), 316. https://doi.org/10.1007/s10661-017-6025-0

Frank, F., McArdell, B. W., Oggier, N., Baer, P., Christen, M., & Vieli, A. (2017). Debris-flow modeling at Meretschibach and Bondasca catchments, Switzerland: Sensitivity testing of field-data-based entrainment model. *Natural Hazards and Earth System Sciences*, *17*(5), 801–815. https://doi.org/10.5194/nhess-17-801-2017

Gaffey, C., & Bhardwaj, A. (2020). Applications of Unmanned Aerial Vehicles in Cryosphere: Latest Advances and Prospects. *Remote Sensing*, *12*(6), Article 6. https://doi.org/10.3390/rs12060948

Ge, H., Xiang, H., Ma, F., Li, Z., Qiu, Z., Tan, Z., & Du, C. (2021). Estimating Plant Nitrogen Concentration of Rice through Fusing Vegetation Indices and Color Moments Derived from UAV-RGB Images. *Remote Sensing*, *13*(9), Article 9. https://doi.org/10.3390/rs13091620

Hagedorn, F., Gavazov, K., & Alexander, J. M. (2019). Above- and belowground linkages shape responses of mountain vegetation to climate change. *Science*, *365*(6458), 1119–1123. https://doi.org/10.1126/science.aax4737

Harsch, M. A., Hulme, P. E., McGlone, M. S., & Duncan, R. P. (2009). Are treelines advancing? A global meta-analysis of treeline response to climate warming. *Ecology Letters*, *12*(10), 1040–1049. https://doi.org/10.1111/j.1461-0248.2009.01355.x

Hendriks, M. (2010). *Introduction to Physical Hydrology*. OUP Oxford.

Henne, P., Elkin, C., Reineking, B., Bugmann, H., & Tinner, W. (2011). Did soil development limit spruce (Picea abies) expansion in the Central Alps during the Holocene? Testing a palaeobotanical hypothesis with a dynamic landscape model. *Journal of Biogeography*, *38*, 933–949. https://doi.org/10.1111/j.1365-2699.2010.02460.x

Holmes, K. W., Griffin, E. A., & van Gool, D. (2021). Digital soil mapping of coarse fragments in southwest Australia: Targeting simple features yields detailed maps. *Geoderma*, *404*, 115282. https://doi.org/10.1016/j.geoderma.2021.115282

Huntington, J. L., Hegewisch, K. C., Daudert, B., Morton, C. G., Abatzoglou, J. T., McEvoy, D. J., & Erickson, T. (2017). Climate Engine: Cloud Computing and Visualization of Climate and Remote Sensing Data for Advanced Natural Resource Monitoring and Process Understanding. *Bulletin of the American Meteorological Society*, *98*(11), 2397–2410. https://doi.org/10.1175/BAMS-D-15-00324.1

Ishwaran, H., Lu, M., & Kogalur, U. (2021). *randomForestSRC: Variable Importance (VIMP) with Subsampling Inference Vignette*. https://doi.org/10.13140/RG.2.2.23799.75680

Jena, R. K., Moharana, P. C., Dharumarajan, S., Sharma, G. K., Ray, P., Deb Roy, P., Ghosh, D., Das, B., Alsuhaibani, A. M., Gaber, A., & Hossain, A. (2023). Spatial Prediction of Soil Particle-Size Fractions Using Digital Soil Mapping in the North Eastern Region of India. *Land*, *12*(7), Article 7. https://doi.org/10.3390/land12071295

Kammer, A., Hagedorn, F., Shevchenko, I., Leifeld, J., Guggenberger, G., Goryacheva, T., Rigling, A., & Moiseev, P. (2009). Treeline shifts in the Ural mountains affect soil organic matter dynamics. *Global Change Biology*, *15*(6), 1570–1583. https://doi.org/10.1111/j.1365-2486.2009.01856.x

Karabadji, N. E. I., Amara Korba, A., Assi, A., Seridi, H., Aridhi, S., & Dhifli, W. (2023). Accuracy and diversity-aware multi-objective approach for random forest construction. *Expert Systems with Applications*, *225*, 120138. https://doi.org/10.1016/j.eswa.2023.120138

Kaya, F., Başayiğit, L., Keshavarzi, A., & Francaviglia, R. (2022). Digital mapping for soil texture class prediction in northwestern Türkiye by different machine learning algorithms. *Geoderma Regional*, *31*, e00584. https://doi.org/10.1016/j.geodrs.2022.e00584

Khedim, N., Cécillon, L., Poulenard, J., Barré, P., Baudin, F., Marta, S., Rabatel, A., Dentant, C., Cauvy-Fraunié, S., Anthelme, F., Gielly, L., Ambrosini, R., Franzetti, A., Azzoni, R. S., Caccianiga, M. S., Compostella, C., Clague, J., Tielidze, L., Messager, E., … Ficetola, G. F. (2021). Topsoil organic matter build-up in glacier forelands around the world. *Global Change Biology*, *27*(8), 1662–1677. https://doi.org/10.1111/gcb.15496

Körner, C. (2021). *Alpine Plant Life: Functional Plant Ecology of High Mountain Ecosystems*. Springer International Publishing. https://doi.org/10.1007/978-3-030-59538-8

Lado, M., Ben-Hur, M., & Shainberg, I. (2004). Soil Wetting and Texture Effects on Aggregate Stability, Seal Formation, and Erosion. *Soil Science Society of America Journal*, *68*(6), 1992–1999. https://doi.org/10.2136/sssaj2004.1992

Li, X., McCarty, G. W., Du, L., & Lee, S. (2020). Use of Topographic Models for Mapping Soil Properties and Processes. *Soil Systems*, *4*(2), Article 2. https://doi.org/10.3390/soilsystems4020032

Ließ, M., Glaser, B., & Huwe, B. (2012). Uncertainty in the spatial prediction of soil texture: Comparison of regression tree and Random Forest models. *Geoderma*, *170*, 70–79. https://doi.org/10.1016/j.geoderma.2011.10.010

Maier, F., van Meerveld, I., Greinwald, K., Gebauer, T., Lustenberger, F., Hartmann, A., & Musso, A. (2020). Effects of soil and vegetation development on surface hydrological properties of moraines in the Swiss Alps. *CATENA*, *187*, 104353. https://doi.org/10.1016/j.catena.2019.104353

Maria Navin, J. R., & Pankaja, R. (2016). Performance Analysis of Text Classification Algorithms using Confusion Matrix. *International Journal of Engineering and Technical Research (IJETR)*. https://d1wqtxts1xzle7.cloudfront.net/54392289/IJETR042741-libre.pdf?1505056014=&response-content-disposition=inline%3B+filename%3DIJETR042741_pdf.pdf&Expires=1699876499&Signature=Qcx5~VemCpDkLfSIzNQDSPpvNKacLIuDQKj9IQSVczuNh9z-MpLTW~mMHlNvfWtik~EKdfWFuHz~ISp0S6G-7h4FczA1wuyQxsffHCa7Ai2kx25NS1vM4i6Tal79jpjknLY2LCxqt3md8QgGNdyRYekV4S~1k0m4buvatDiu88nWkP4EmH4AYh2TS3asyG-Yy7gxbp0MBNUV~oNKnL9BRKnweSU2Ox1xjvLkGc3C~mUdXOjypqt6bXcUxooV7ZfVYas6bDiQm0AFm7l5M4vX3jXoMD3pa4a~eetkqNRxPeYlCs8pxbx9dWoSLbA7OrN-JLFNHvq5z3~0xf3i6kwcRQ__&Key-Pair-Id=APKAJLOHF5GGSLRBV4ZA

Mazzotti, G., Webster, C., Essery, R., & Jonas, T. (2021). Increasing the Physical Representation of Forest-Snow Processes in Coarse-Resolution Models: Lessons Learned From Upscaling Hyper-Resolution Simulations. *Water Resources Research*, *57*(5), e2020WR029064. https://doi.org/10.1029/2020WR029064

McKenzie, N. J., & Ryan, P. J. (1999). Spatial prediction of soil properties using environmental correlation. *Geoderma*, *89*(1), 67–94. https://doi.org/10.1016/S0016-7061(98)00137-2

Moore, I. D., & Burch, G. J. (1986). Physical Basis of the Length-slope Factor in the Universal Soil Loss Equation. *Soil Science Society of America Journal*, *50*(5), 1294–1298. https://doi.org/10.2136/sssaj1986.03615995005000050042x

Moore, I. D., Gessler, P. E., Nielsen, G. A., & Peterson, G. A. (1993). Soil Attribute Prediction Using Terrain Analysis. *Soil Science Society of America Journal*, *57*(2), 443–452. https://doi.org/10.2136/sssaj1993.03615995005700020026x

Myers-Smith, I. H., & Hik, D. S. (2017, June 9). *Climate warming as a driver of tundra shrubline advance—Myers-Smith—2018—Journal of Ecology—Wiley Online Library*. https://besjournals.onlinelibrary.wiley.com/doi/full/10.1111/1365-2745.12817

Odeh, I. O. A., McBratney, A. B., & Chittleborough, D. J. (1995). Further results on prediction of soil properties from terrain attributes: Heterotopic cokriging and regression-kriging. *Geoderma*, *67*(3), 215–226. https://doi.org/10.1016/0016-7061(95)00007-B

Özkan, K., Mert, A., & Özdemir, S. (2023). A new proposed GLCM texture feature: Modified Rényi Deng entropy. *The Journal of Supercomputing*, *79*(18), 21507–21527. https://doi.org/10.1007/s11227-023-05627-z

Oztas, T., & Fayetorbay, F. (2003). Effect of freezing and thawing processes on soil aggregate stability. *CATENA*, *52*(1), 1–8. https://doi.org/10.1016/S0341-8162(02)00177-7

Pahlavan-Rad, M. R., Dahmardeh, K., Hadizadeh, M., Keykha, G., Mohammadnia, N., Gangali, M., Keikha, M., Davatgar, N., & Brungard, C. (2020). Prediction of soil water infiltration using multiple linear regression and random forest in a dry flood plain, eastern Iran. *CATENA*, *194*, 104715. https://doi.org/10.1016/j.catena.2020.104715

Partio, M., Cramariuc, B., Gabbouj, M., & Visa, A. (2002). *Rock texture retrieval using gray level co-occurrence matrix*.

Peters, J., Baets, B. D., Verhoest, N. E. C., Samson, R., Degroeve, S., Becker, P. D., & Huybrechts, W. (2007). Random forests as a tool for ecohydrological distribution modelling. *Ecological Modelling*, *207*(2), 304–318. https://doi.org/10.1016/j.ecolmodel.2007.05.011

Pouladi, N., Møller, A. B., Tabatabai, S., & Greve, M. H. (2019). Mapping soil organic matter contents at field level with Cubist, Random Forest and kriging. *Geoderma*, *342*, 85–92. https://doi.org/10.1016/j.geoderma.2019.02.019

Prasad, A. M., Iverson, L. R., & Liaw, A. (2006). Newer Classification and Regression Tree Techniques: Bagging and Random Forests for Ecological Prediction. *Ecosystems*, *9*(2), 181–199. https://doi.org/10.1007/s10021-005-0054-1

Ramsankaran, R., Navinkumar, P. J., Dashora, A., & Kulkarni, A. V. (2021). UAV-Based Survey of Glaciers in Himalayas: Challenges and Recommendations. *Journal of the Indian Society of Remote Sensing*, *49*(5), 1171–1187. https://doi.org/10.1007/s12524-020-01300-7

Revuelto, J., Alonso-Gonzalez, E., Vidaller-Gayan, I., Lacroix, E., Izagirre, E., Rodríguez-López, G., & López-Moreno, J. I. (2021). Intercomparison of UAV platforms for mapping snow depth distribution in complex alpine terrain. *Cold Regions Science and Technology*, *190*, 103344. https://doi.org/10.1016/j.coldregions.2021.103344

Rumpf, S. B., Gravey, M., Brönnimann, O., Luoto, M., Cianfrani, C., Mariethoz, G., & Guisan, A. (2022). From white to green: Snow cover loss and increased vegetation productivity in the European Alps. *Science*, *376*(6597), 1119–1122. https://doi.org/10.1126/science.abn6697

Salim, E., Ravanel, L., Bourdeau, P., & Deline, P. (2021). Glacier tourism and climate change: Effects, adaptations, and perspectives in the Alps. *Regional Environmental Change*, *21*(4), 120. https://doi.org/10.1007/s10113-021-01849-0

Skaling, W. (2008). *FOR OVER 50 YEARS, INNOVATIVE INSTRUMENTS BUILT ON UNDERSTANDING SOIL, WATER AND PLANTS*.

Soil Survey Manual 2017. (n.d.).

Song, J., Gao, Y., Yin, P., Li, Y., Li, Y., Zhang, J., Su, Q., Fu, X., & Pi, H. (2021). The Random Forest Model Has the Best Accuracy Among the Four Pressure Ulcer Prediction Models Using Machine Learning Algorithms. *Risk Management and Healthcare Policy*, *14*, 1175–1187. https://doi.org/10.2147/RMHP.S297838

Steinbauer, M. J., Grytnes, J.-A., Jurasinski, G., Kulonen, A., Lenoir, J., Pauli, H., Rixen, C., Winkler, M., Bardy-Durchhalter, M., Barni, E., Bjorkman, A. D., Breiner, F. T., Burg, S., Czortek, P., Dawes, M. A., Delimat, A., Dullinger, S., Erschbamer, B., Felde, V. A., … Wipf, S. (2018). Accelerated increase in plant species richness on mountain summits is linked to warming. *Nature*, *556*(7700), Article 7700. https://doi.org/10.1038/s41586-018-0005-6

Sturm, M., Holmgren, J., McFadden, J. P., Liston, G. E., Chapin, F. S., & Racine, C. H. (2001). Snow–Shrub Interactions in Arctic Tundra: A Hypothesis with Climatic Implications. *Journal of Climate*, *14*(3), 336–344. https://doi.org/10.1175/1520-0442(2001)014<0336:SSIIAT>2.0.CO;2

Takoutsing, B., & Heuvelink, G. B. M. (2022). Comparing the prediction performance, uncertainty quantification and extrapolation potential of regression kriging and random forest while accounting for soil measurement errors. *Geoderma*, *428*, 116192. https://doi.org/10.1016/j.geoderma.2022.116192

van de Lisdonk, D. (2023). *Hydraulic and physical properties of alpine soils in relation to terrain and vegetation*.

Velde, B. B., & Meunier, A. (2008). *The Origin of Clay Minerals in Soils and Weathered Rocks*. Springer Science & Business Media.

Veronesi, F., & Schillaci, C. (2019). Comparison between geostatistical and machine learning models as predictors of topsoil organic carbon with a focus on local uncertainty estimation. *Ecological Indicators*, *101*, 1032–1044. https://doi.org/10.1016/j.ecolind.2019.02.026

Viviroli, D., Archer, D. R., Buytaert, W., Fowler, H. J., Greenwood, G. B., Hamlet, A. F., Huang, Y., Koboltschnig, G., Litaor, M. I., Lopez-Moreno, J. I., Lorentz, S., Schaedler, B., Schreier, H., Schwaiger, K., Vuille, M., & Woods, R. (2011). Climate change and mountain water resources: Overview and recommendations for research, management and policy. *Hydrology and Earth System Sciences*, *15*(2), 471–504. https://doi.org/10.5194/hess-15-471-2011

Viviroli, D., Kummu, M., Meybeck, M., Kallio, M., & Wada, Y. (2020). Increasing dependence of lowland populations on mountain water resources. *Nature Sustainability*, *3*(11), Article 11. https://doi.org/10.1038/s41893-020-0559-9

Xu, C., Li, Y., Hu, J., Yang, X., Sheng, S., & Liu, M. (2012). Evaluating the difference between the normalized difference vegetation index and net primary productivity as the indicators of vegetation vigor assessment at landscape scale. *Environmental Monitoring and Assessment*, *184*(3), 1275–1286. https://doi.org/10.1007/s10661-011-2039-1

Yang, R., Hong, C., Liu, W., Wu, X., Wang, T., & Huang, Z. (2021). Non-contaminating cryogenic fluid access to high-temperature resources: Liquid nitrogen fracturing in a lab-scale Enhanced Geothermal System. *Renewable Energy*, *165*, 125–138. https://doi.org/10.1016/j.renene.2020.11.006

Zhou, J., Lai, L., Guan, T., Cai, W., Gao, N., Zhang, X., Yang, D., Cong, Z., & Zheng, Y. (2016). Comparison modeling for alpine vegetation distribution in an arid area. *Environmental Monitoring and Assessment*, *188*(7), 408. https://doi.org/10.1007/s10661-016-5417-x

8 APPENDIX

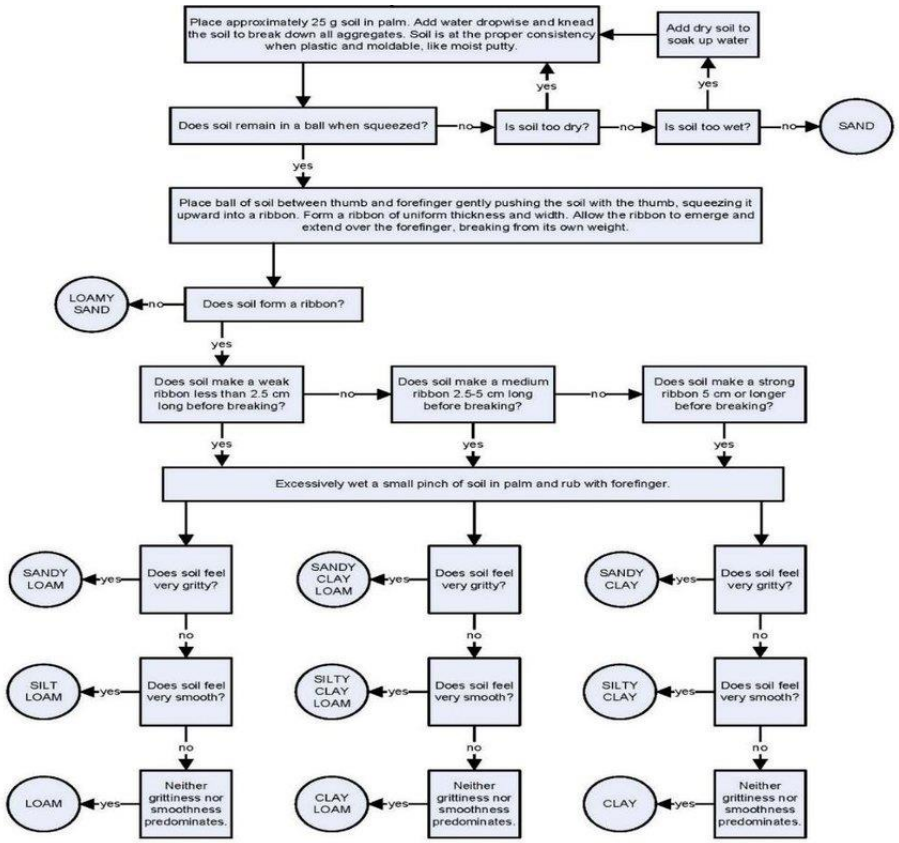

Appendix 1: protocol to classify the soil texture in-field estimation

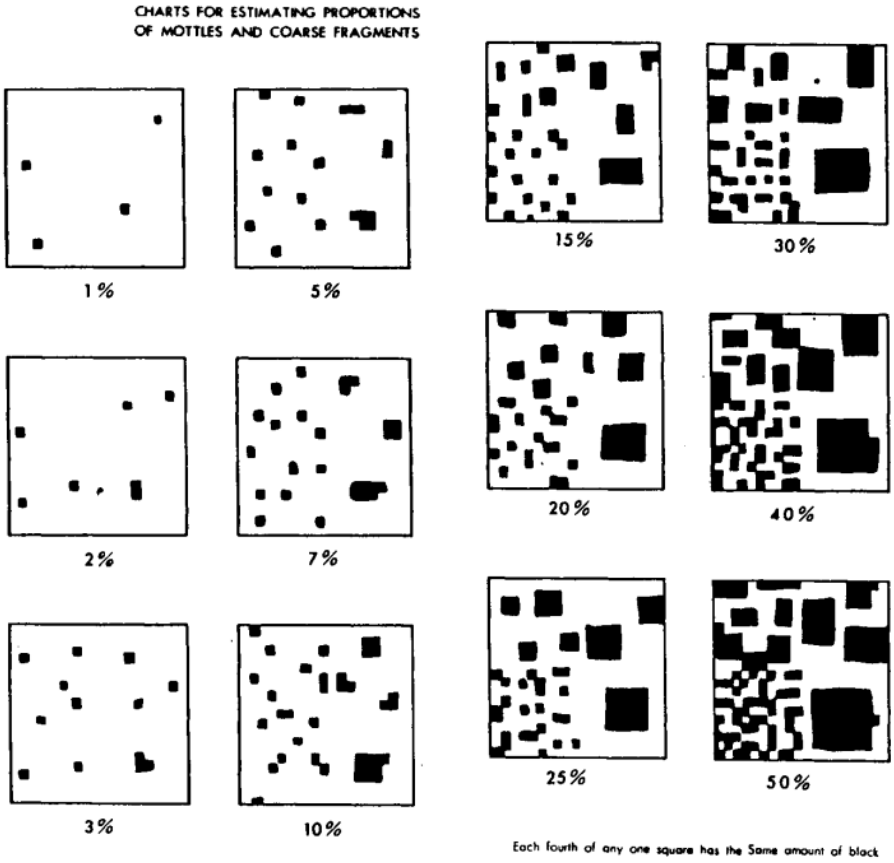

Appendix 2: Estimation diagram of rock size and percentages for in-field estimation.

Topography property	How to characterize	How to measure
Slope	Use the in-field tool to estimate the slope angle.	Estimation of slope in degrees and classify the slope.
Aspect	Use the compass to assess the aspect of the slope	Estimation of the major wind direction of the slope.

Appendix 3: Protocol for the in-field measurements of the topography properties.

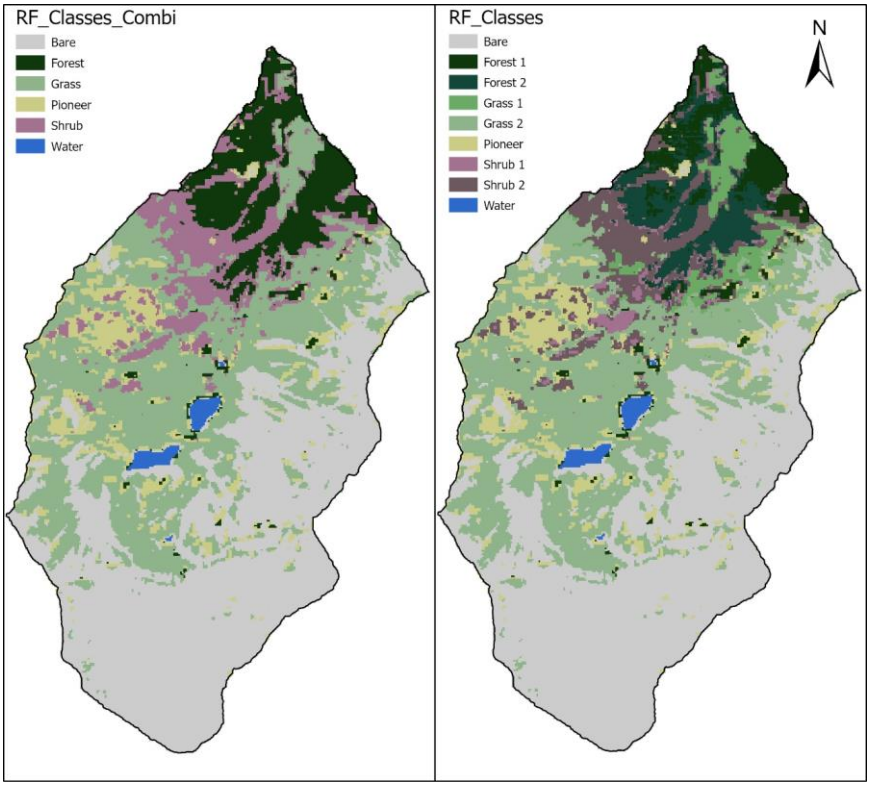

Appendix 4: RF model vegetation classification based on Sentinel-2 imagery attributes only

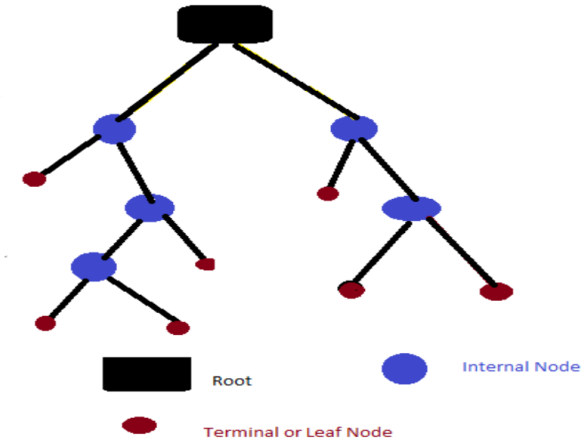

Appendix 5: Decision Tree structure, image obtained from Ali et al. (2012)

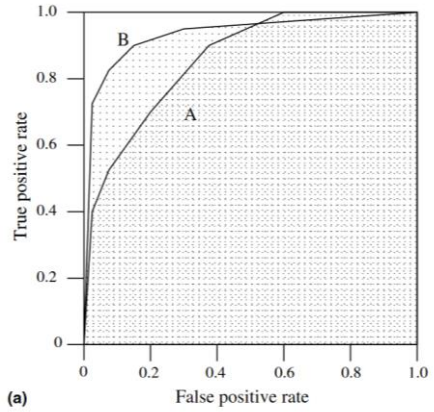

Appendix 6: ROC graph shows the area under two ROC curves (A) and (B). Image adjusted from Fawcett (2006)

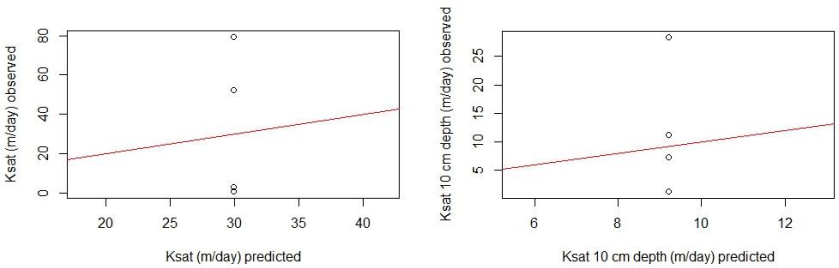

Appendix 7: Ksat plots, left plot representing the surface plot and right plot on 10 cm depth.

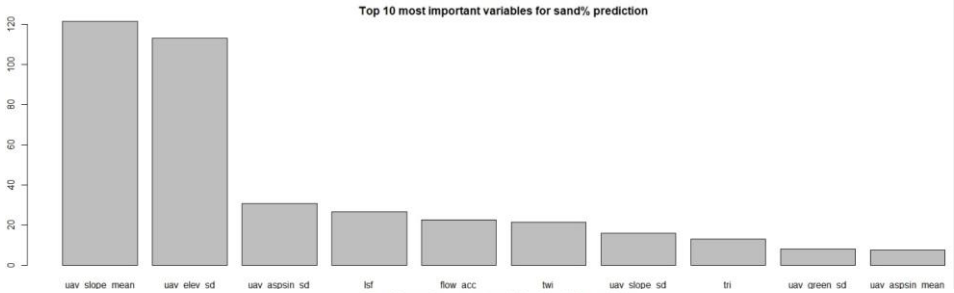
Top 10 most important variables for sand% prediction
0
20
40
60
80
100
120
uav_slope_mean
uav_elev_sd
uav_aspsin_sd
lsf
flow_acc
twi
uav_slope_sd
tri
uav_green_sd
uav_aspsin_mean

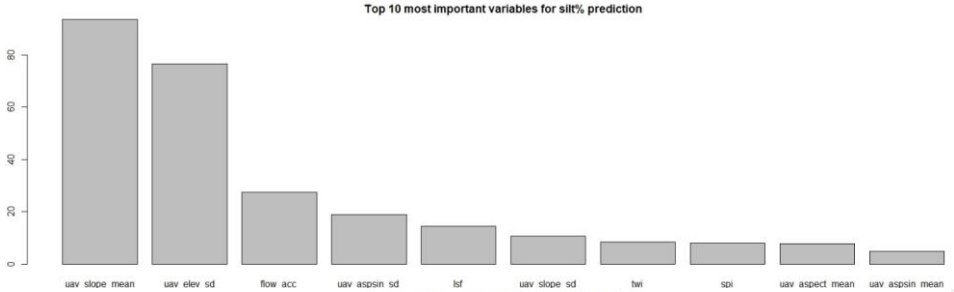
Top 10 most important variables for silt% prediction
0
20
40
60
80
uav_slope_mean
uav_elev_sd
flow_acc
uav_aspsin_sd
lsf
uav_slope_sd
twi
spi
uav_aspect_mean
uav_aspsin_mean

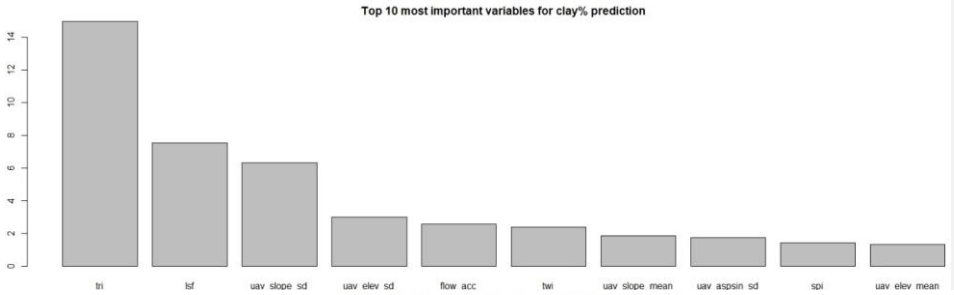
Top 10 most important variables for clay% prediction
0
2
4
6
8
10
12
14
tri
lsf
uav_slope_sd
uav_elev_sd
flow_acc
twi
uav_slope_mean
uav_aspsin_sd
spi
uav_elev_mean

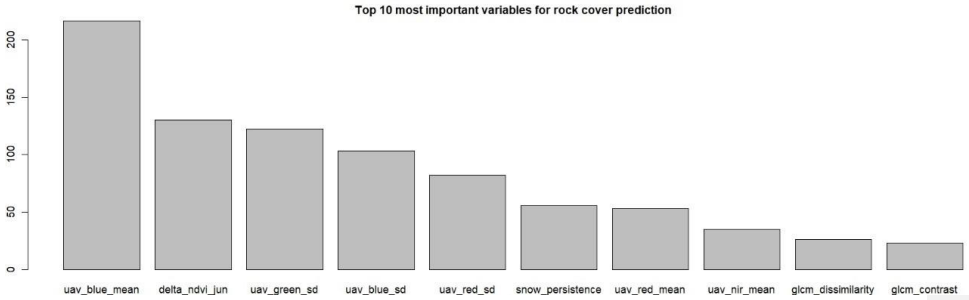
Top 10 most important variables for rock cover prediction
0
50
100
150
200
uav_blue_mean
delta_ndvi_jun
uav_green_sd
uav_blue_sd
uav_red_sd
snow_persistence
uav_red_mean
uav_nir_mean
glcm_dissimilarity
glcm_contrast

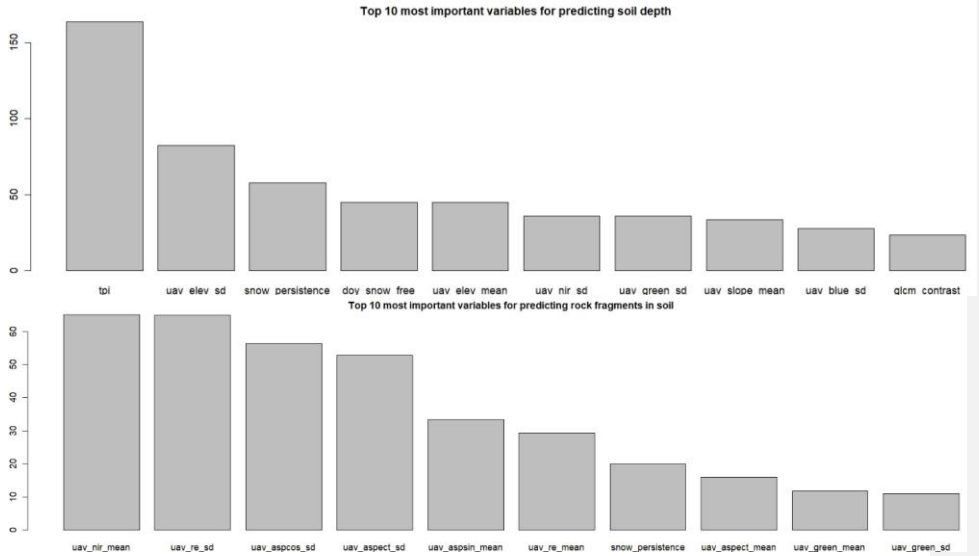

Appendix 8: Top 10 most important variables for soil textural factors, for rock cover percentage, rock fragments in soil and soil depth.

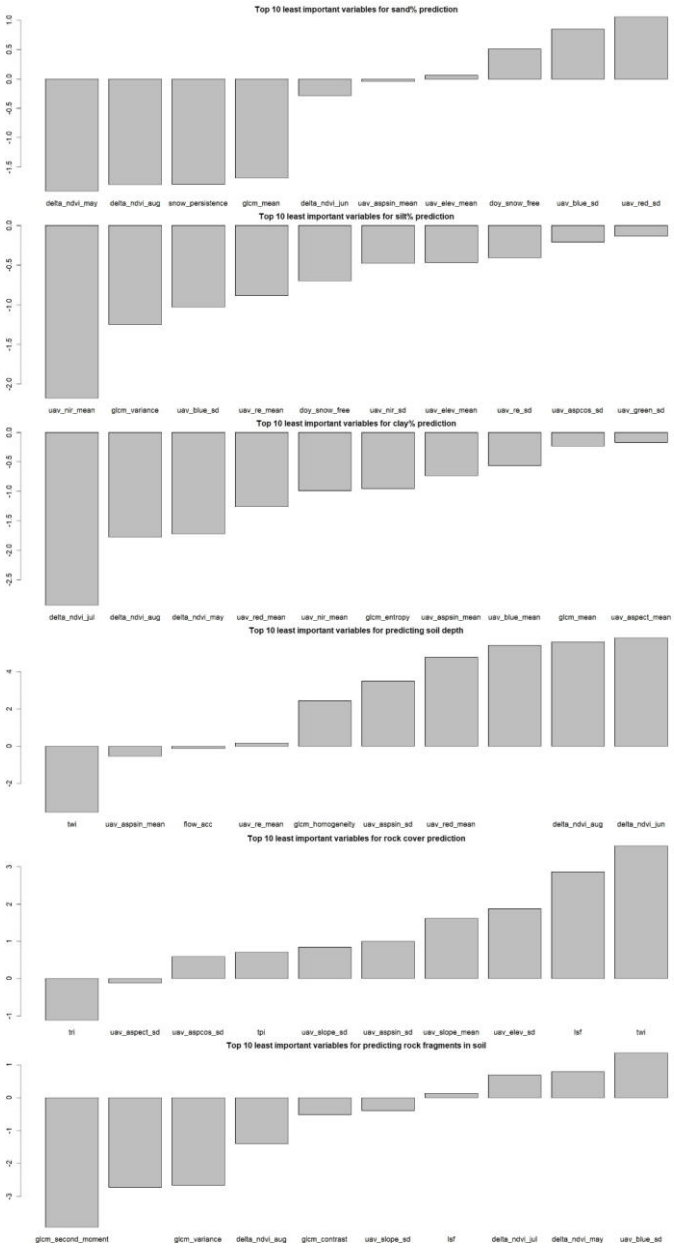

Appendix 9: Top 10 least important variables for regression predictions

Appendix 10: Accuracies for scenario 2 and 3

$RMSE_2$	$RMSE_3$	(OOB) R^2_2	(OOB) R^2_3
10.5	10.0	0.018	0.005
10.7	11.0	0.075	0.023
11.0	11.2	0.068	0.027
14.5	14.7	0.60	0.58
17.3	17.7	-0.032	-0.060
19.9	20.6	0.084	0.081
x	x	x	x
x	x	x	x

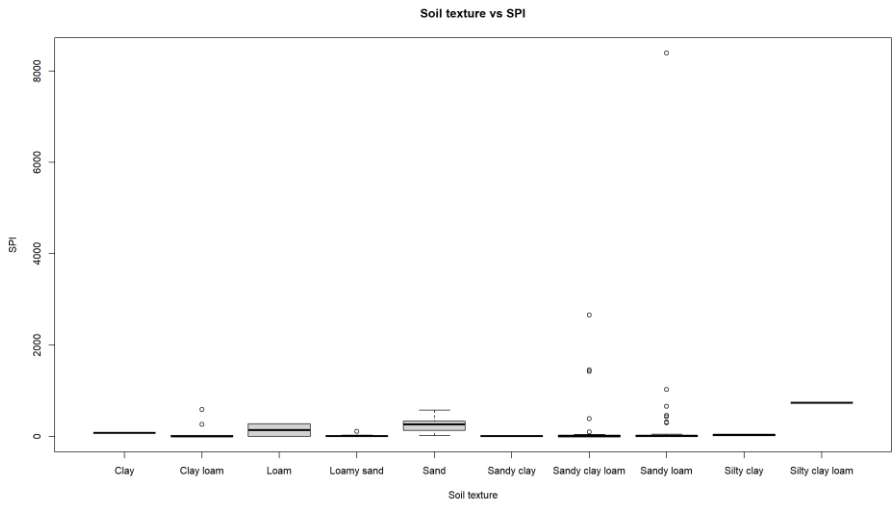

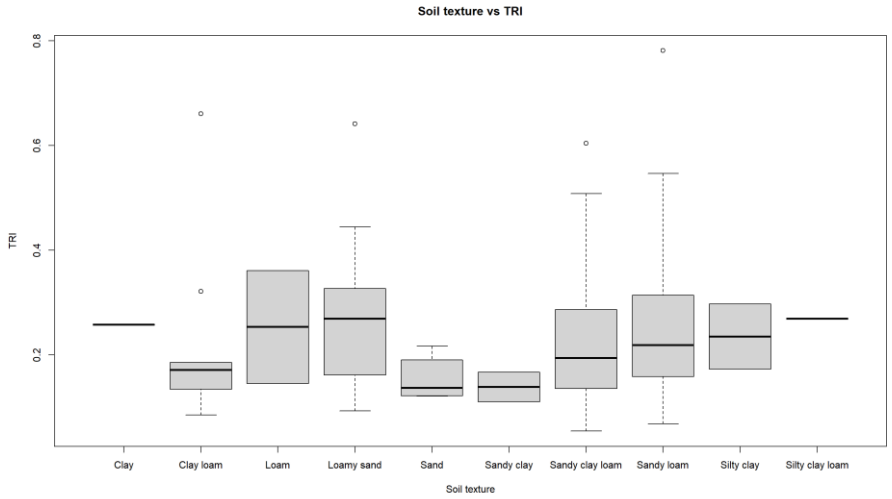

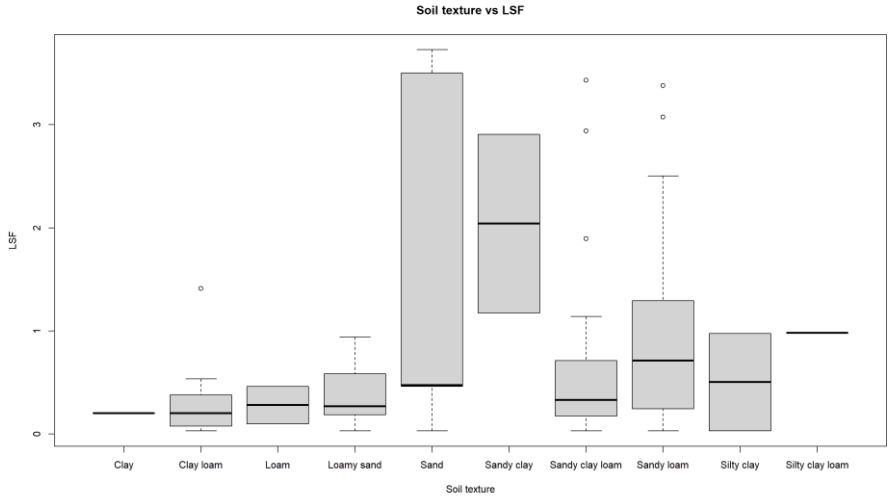

Appendix 11: soil texture vs erosional features

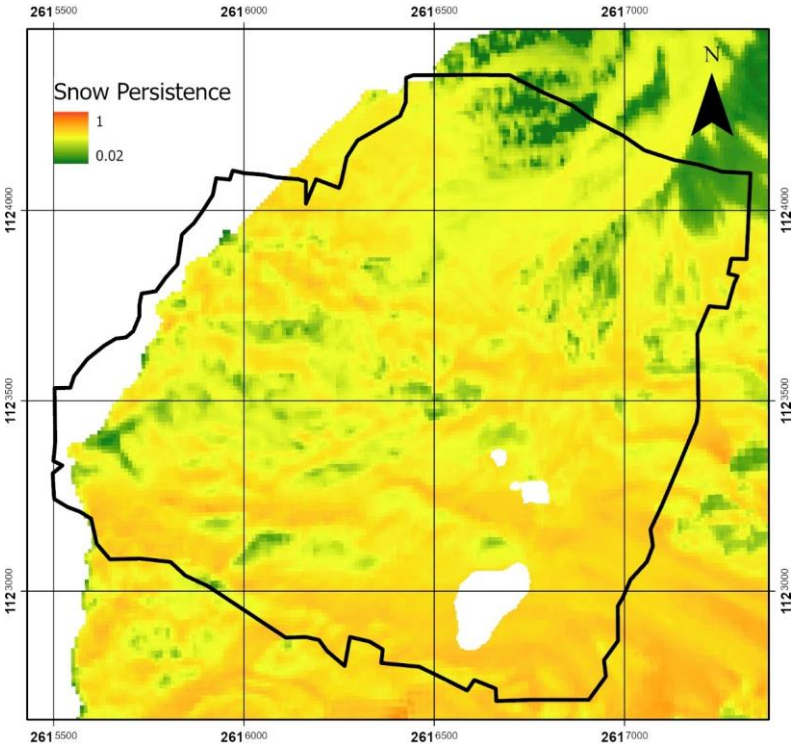

Appendix 12: Snow persistence map

Confusion matrix:

observed	predicted Clay	Clay loam	Loam	Loamy sand	Sand	Sandy clay	Sandy clay loam
Clay	0	0	0	0	0	0	0
Clay loam	0	0	0	3	0	0	2
Loam	0	0	0	0	0	0	0
Loamy sand	0	1	0	0	0	0	4
Sand	0	0	0	1	2	0	0
Sandy clay	0	0	0	0	0	0	0
Sandy clay loam	0	0	0	1	0	0	6
Sandy loam	0	0	0	3	0	0	6
Silty clay	0	0	0	0	0	0	0
Silty clay loam	0	0	0	0	0	0	0

observed	predicted Sandy loam	Silty clay	Silty clay loam	class.error
Clay	1	0	0	1.0000
Clay loam	5	0	0	1.0000
Loam	2	0	0	1.0000
Loamy sand	12	0	0	1.0000
Sand	2	0	0	0.6000
Sandy clay	2	0	0	1.0000
Sandy clay loam	18	0	0	0.7600
Sandy loam	34	0	0	0.2093
Silty clay	2	0	0	1.0000
Silty clay loam	1	0	0	1.0000

Appendix 13: Confusion matrix of RF classfication model of soil texture prediction

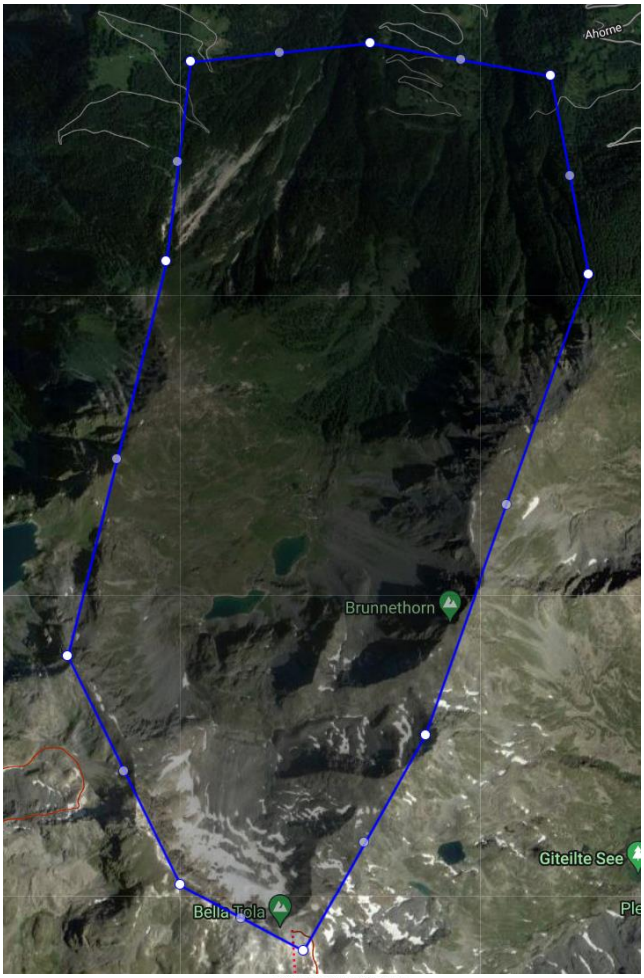
Ahorne
Brunnethorn
Giteilte See
Bella Tola

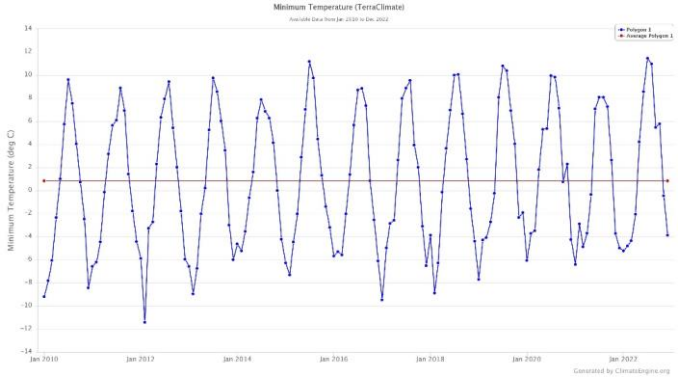
Minimum Temperature (TerraClimate)
Minimum Temperature (deg C)
Jan 2010
Jan 2012
Jan 2014
Jan 2016
Jan 2018
Jan 2020
Jan 2022

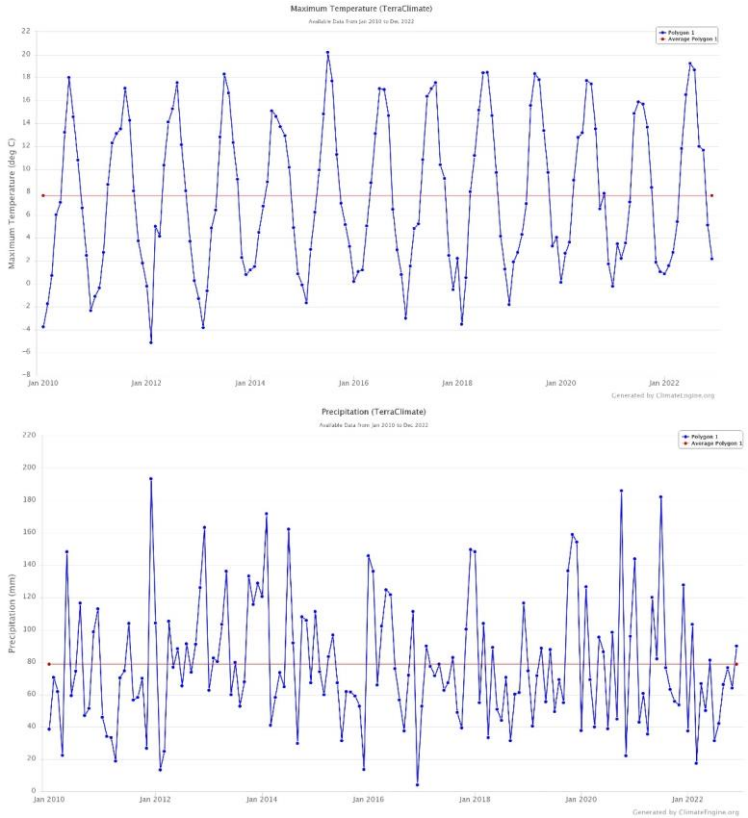

Appendix 14: Climate information derived from climateengine.org, polygon was drawn and from the polygon precipitation and temperature information was derived from the TerraClimate dataset (Huntington et al., 2017).